Translational control as a novel regulator of gradient sensing and chemotropism in yeast

Rita Gelin-Licht[1,2], Patrick J. Conlon[2], Raman Singh[1], Rohini R. Nair[1], Camila Baez[1], Lihi Gal[1], Maya Schuldiner[1], Andre Levchenko[2,3,4], and Jeffrey E. Gerst[1,3,5]

[1]Department of Molecular Genetics, Weizmann Institute of Science
Rehovot 7610001, Israel

[2]Department of Biomedical Engineering, Yale University, New Haven, CT USA

[3]Co-corresponding authors

[4]Tel: +1-410-949-5944
Email: andre.levchenko@yale.edu

[5]Tel: +972-8-9342106
Fax: +972-8-9344108
Email: jeffrey.gerst@weizmann.ac.il

Keywords: chemotropism, yeast mating pathway, gradient sensing, cell fusion, G-protein coupled receptor, MAP kinase, Scp160, Asc1, Gpa2, Gpa1, ribosomal proteins, ribosome specialization, paralog specificity, translation, yeast

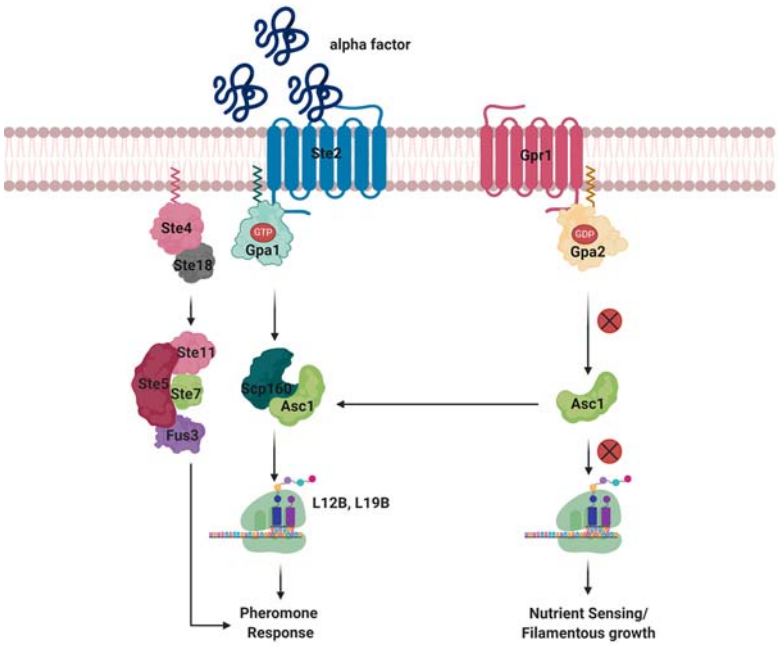

Abstract

The yeast mating pathway regulates haploid cell fusion to form diploids in response to pheromone signaling. Study of this pathway has led to important insights into the structure and function of mitogen-activated protein kinase (MAPK) cascades, yet our understanding of how external signals are converted into specific changes in gene expression and cell morphology is incomplete. For example, the regulators of directional growth (chemotropism) remain poorly defined. Upon pheromone exposure, yeast grow asymmetrically towards a nearby mating partner (chemotropic morphogenesis) and form a mating projection (shmoo). Using non-biased genome-wide screening, we identify >20 novel positive and negative regulators of pheromone gradient sensing, shmoo development, and mating. In addition to known regulators of exocytic and endocytic pathways, several are directly involved in translational control downstream of the G-protein-regulated pheromone and filamentous growth MAPK pathways. These include the Scp160 RNA-binding protein and ribosomal proteins Asc1, Rpl12b and Rpl19b. Importantly, pheromone treatment and Gα (Gpa1) activation both stimulate Scp160 binding to, and inhibition of, Asc1, which acts downstream of glucose-activated Gα (Gpa2) on the filamentous growth pathway. We also identify Rpl12b and Rpl19b as paralog-specific positive regulators of translation of specific mating pathway components, including Scp160. Thus, the different MAPK pathways converge at the level of translational control to regulate signaling.

Introduction

For cells to communicate and coordinate activities, both single- and multi-cellular systems have evolved signaling networks to transduce and amplify input signals, and transform them into phenotypic responses. Such responses include the ability of cells to grow or migrate towards the source of a signal and support specific cell-cell interactions (*e.g.* cell fusion, axon guidance and connectivity) or confer immune responsiveness. Yet, despite extensive study, these processes are not fully understood and the consequences of inappropriate activation or inhibition of such signaling pathways, as well as the relationship between input signals (*e.g.* hormone[1], drug[2], or growth factor[3]) and output signals (*e.g.* synaptic function[4] or metastatic invasion[5]), including those related to human disease (*e.g.* cancer, neurodegeneration) etiology, have not been fully elucidated.

Both chemotropism (directional growth towards an extracellular stimulus)[6-9] and chemotaxis (directional migration towards an extracellular stimulus)[10-12] are responses frequently controlled by G-protein coupled-receptor (GPCR) signaling, leading to the activation of mitogen-associated protein kinase (MAPK) networks[13-15]. The cellular mechanisms that underlie these processes are also not fully characterized. The yeast, *S. cerevisiae*, which senses and responds chemotropically to mating pheromone via MAPK signaling[9, 16] is an ideal system in which to study chemotropism. Discovery of the mating and other MAPK signaling pathways in yeast led to the identification of homologous signaling networks in mammalian cells, principally due to the high degree of genetic and biochemical conservation.

A pheromone-activated MAPK cascade allows *MAT*a and *MAT*α haploid yeast cells to respond to pheromone secreted by the opposite mating type to confer the cessation of cell proliferation, polarized chemotropic growth in the direction of the pheromone gradient, and ultimately cell-cell fusion[17]. Pheromone binding to mating type-specific GPCRs activates the Gα-subunit (Gpa1) and G$\beta\gamma$ subunit dimer (Ste4/Ste18) in both mating types[17, 18]. Upon activation, Gα undergoes GDP-GTP exchange and dissociates from G$\beta\gamma$ to initiate events that precede mating, including gene transcription, cell cycle arrest, as well as the morphological and cytoskeletal changes necessary for mating[9, 17, 18]. In addition to signaling via G$\beta\gamma$, a separate signaling function for Gα/Gpa1 occurs via Scp160[19], a KH domain-containing RNA-binding protein (RBP)[20]. We have previously shown that RNA-binding by Scp160 is stimulated by pheromone treatment (or direct Gpa1 activation) and delivers mRNAs encoding components of the pheromone-activated MAPK cascade to the site of mating projection (shmoo) formation[21]. Scp160-dependent mRNA delivery to the shmoo tip occurs via directed cortical endoplasmic reticulum (cER) movement and is

necessary for continuous correction of the growth of the mating projection[21], as temporal and spatial accuracy is required for the successful fusion between partners[9, 16]. Thus, Scp160 contributes to chemotropic growth by targeting specific mRNAs to the site of polarization to mediate both gradient sensing, as well as temporal and spatial growth responses to the gradient[21].

Given the paucity of information regarding how chemotropic growth is specifically controlled, we employed non-biased high-throughput screening of yeast gene deletion and DAmP libraries to identify genes, which, when mutated, specifically affect chemotropism (and not other processes involved in mating). Using this approach we identified over 20 novel positive and negative regulators of chemotropism. While many are associated with exocytosis and endocytosis, which are important for the direct trafficking of pheromone receptors and agglutinins required for mating, we also identify genes involved in translational control. Importantly, we demonstrate that Scp160 function and its role in chemotropic growth is inhibited by Asc1, a 40S ribosomal protein (RP) that is an ortholog of mammalian RACK1[13, 22]. In yeast, Asc1 is involved in the invasive growth response to nutrient limitation via the Gα (Gpa2)-activated MAPK cascade[23, 24]. Although earlier work suggested that Asc1 interacts preferentially with the inactive GDP-bound form of Gpa2, it is nevertheless required for invasive growth[25]. Earlier studies also found that Asc1 facilitates Scp160 binding to ribosomes, indicating a role in the translation of Scp160-bound messages[26]. In addition, Asc1 associates with proteins directly involved in translation initiation (*e.g.* Nip1, Rgp1)[27, 28] and is essential for translation initiation at elevated temperatures[29].

Here we not only identify a bilateral relationship between Scp160 and Asc1, we show that Scp160 physically binds Asc1 upon pheromone signaling, but not during nutrient signaling. We also demonstrate that specific ribosomal protein (RP) paralogs are required for the translation of proteins involved in chemotropism and mating. Thus, this study shows that chemotropism is directly regulated by translational control and that the different MAPK pathways (*e.g.* pheromone-activated mating pathway and nutrient-activated filamentous growth pathway) buffer each other's responses to upstream signaling.

Results

A screen for positive and negative regulators of yeast cell mating

Deficiencies in yeast cell mating can result from a number of reasons, including: an inability to initiate polarized growth in response to pheromone; failure to sense the pheromone gradient; and defects in either cell wall remodeling or cell-cell fusion[30-32]. To select for mutants specifically defective in gradient sensing and chemotropism, we developed a genetic screening approach to first identify strains deficient in mating and then, specifically, those defective in chemotropic growth.

We first employed high-throughput screening of yeast mutant gene libraries to identify genes involved in mating *per se.* To do this we devised an imaging-based approach to systematically evaluate the mating efficiency for individual gene mutants. The working principle involved mating yeast mutant strains to wild-type (WT) cells and employing image-based detection of both haploids (*i.e.* non-mated cells) and fused zygotes (*i.e.* mated cells) to quantify the overall mating efficiency of the mutant (Figure 1A). To apply this in a high-throughput format, we utilized a pinning robot to mate a WT strain in high density format[33] to gene knockout[34] and hypomorphic allele (DAmP)[35] libraries, which automated haploid cell mixing, mating, and imaging. To increase the visual ability to detect mating events, the knockout library was manipulated to express a cytosolic mCherry reporter (Figure 1A). In order to assess mating efficiency, the *MAT*a mCherry library strains were mixed with GFP-expressing *MAT*α WT cells on agar, after which the mating mixtures were collected, fixed, and imaged. After segregating the mCherry and GFP channel images, the number of mated and unmated cells were counted, and a mating fraction metric was used to assess mating efficiency for each mutant. Overall, the mating efficiencies of 5,131 mutants (*e.g.* 4,357 knockouts and 774 DAmP mutants of essential genes) were evaluated in the screen out of the ~5,800 total genes in the yeast genome (Figure 1B). We note that ~600 mutants were missing from the screen. These included yeast deleted for genes vital for mating (*i.e.* most *STE* genes and *SCP160*) or cell growth, as the inability to mate/proliferate prevented these strains from completing library creation.

Image analysis of the mutants (Table S1; sheet – *Primary screen*) suggested that ~740 genes may either regulate or affect mating efficiency, based upon the fraction of cells that underwent mating (Figure 1C and Table S1, sheet – *Selected genes*). We note that WT BY4741 cells show a range in mating from 36-51% of the population (Figure 1C). Other genes, including those not specific to mating (*e.g.* mitochondrial and non-specific transcription, translation, and metabolic genes), were not included in this group. To validate the reliability of the primary screen,

a second automated screen was performed with this select group of genes applying the same conditions (Table S1, sheet – *Selected*). We found that screen reproducibility was very high (>95.8%) in that positive or negative regulators from the first screen had similar results in the second relative to the controls.

Mutants of positive regulators (*i.e.* genes known to be important for mating) showed severe mating defects (*e.g.* scoring at the bottom 10% of mating efficiency). These included known genes such as *STE13*, *STE50*, *FUS3*, and *CDC42* (Figure 2A). The list of positive regulators also included previously characterized genes, like those encoding components of the exocyst (*e.g. SEC3, SEC10, SEC15, EXO84*) that is involved in secretion, but was not known to mediate chemotropism *per se*[9, 36, 37]. In contrast, mutants of negative regulators (*e.g.* genes known to be antagonistic to the mating pathway) showed highly proficient mating (*i.e.* top 5% of mating efficiency). These included genes such as *HOG1*, *PBS2*, *GPA2,* and *GPR1* (Figure 2C). Both *GPR1* and *GPA2* encode proteins (*i.e.* the GPCR and Gα, respectively) involved in glucose sensing and cell cycle progression[23, 24, 38, 39], while *HOG1* and *PBS2* encode proteins in MAPK cascade involved in the cellular response to high osmolarity conditions[40]. In addition to these known (or more obvious) genes, others were identified that have not been described in the context of mating, including uncharacterized ORFs identified as positive regulators (*e.g. YML089c, YML083C, YML082W*, which occupy a common region in Chr. XIII adjacent to *TUB1* and might affect its expression), as well as *SFD1*.

From these validated results, we further evaluated 49 positive and negative regulators of mating, as well as 17 potential positive regulators missing from the first screen because of their inability to mate. We performed manual deletion of non-essential genes (52 genes) and used a tetracycline-repressible (tet-off) promoter system[41] for essential genes (*e.g. SEC10, SEC15, EXO84, BUL3, YPP1,* and *TRS31*) (14 genes) (Table S1, sheet – *Manual validation, column C*). Manual validation (66 genes total) was used to verify that the mating phenotype obtained from screening corresponded to the correct gene mutation in the query strain. We performed quantitative mating assays in crosses against WT cells (Figures 2C and D). We also included a negative control, *cdc24-m3*, which contains a recessive mutation in the exchange factor for the Cdc42 GTPase and is severely inhibited in chemotropism and mating[42]. The results obtained from manual manipulation were in high (>83%) qualitative agreement with the results of the library screen (Figure 1C and Table S1) and showed a varying degree in the regulation of mating. This was true for both positive (Figure 2C) and negative regulators (Figure 2D) of mating. Among mutants not present in the initial screen, but examined manually, we found that 80% positively regulated mating, while 12%

behaved as wild-type cells and 8% exhibited negative regulation of mating (Figure 2B,D and Table S1, sheet – *Manual validation*).

A screen for positive and negative regulators of chemotropism

To assess the specific contribution of candidate genes to chemotropism, we performed an additional type of screen called the "pheromone confusion" technique or assay[43]. The confusion assay compares the mating efficiency of *MAT*a and *MAT*α haploid cells either with or without exogenous α-factor added to the mating mixture (Figure 3A). The mating efficiency of WT cells is significantly reduced when exogenous α-factor is present because WT *MAT*a cells are no longer able to detect the pheromone gradient coming from their *MAT*α partner. However, mutant *MAT*a cells that have a defect in chemotropism do not show any further reduction in mating efficiency when the gradient is disrupted by added α-factor.

To evaluate their chemotropic properties, we determined the mating efficiency of 42 manually validated positive regulators either with or without added pheromone (Figure 3B and Table S1, sheet – *Manual validation, columns D and E*). We did not examine deletions of the negative regulators of mating since they are already likely to be indifferent to external pheromone. We found a number of gene deletions to be highly deficient in chemotropism in the confusion assay, since they exhibited no further decrease in mating efficiency upon exposure to exogenous pheromone at saturating concentrations, relative to untreated cells (Figure 3B). In contrast, the mating efficiency of WT control cells was greatly inhibited by the exogenous addition of pheromone (Figure 3B). We identified this group of mutants as novel chemotropism-related candidates (*i.e. sec3Δ, sec10, sec15, exo84, trs31, ypp1, bul3, ahk1Δ, bem4, sfd1Δ, rax1Δ,* and *scp160Δ*). This group also includes *scp160KHΔ14*, an allele which lacks the last KH RNA-binding domain of Scp160 and is unable to bind RNA[44], and the *cdc24-m3* allele, as controls.

Quantitation of MAPK activity via Fus1 signaling and shmoo formation

To help understand how these different genes affect chemotropism and mating, we quantified both the signaling and morphological responsiveness to pheromone stimulation of both the chemotropism mutants and negative regulators of mating (*i.e. hog1Δ, ygr016wΔ, ska1Δ, irc19Δ, gpr1Δ, yml053cΔ, ira2Δ, asc1Δ*). We determined the relationship between defects in gradient sensing and activity of the MAPK pathway in the different strains using Fus1-GFP as a reporter[45]. In parallel, we examined shmoo formation as an indicator of readout at the morphological level. By employing flow cytometry, Fus1-GFP expression levels (Figure 4A) and shmoo projection

formation (Figure 4B) were assayed. Mutants in positive regulators (*e.g. scp160Δ*, *sec15*, *bul3Δ*, *ahk1Δ*) demonstrated reduced Fus1 expression in parallel with poor shmoo formation in all cases (Figures 4A and B; left panels). Positive controls in this experiment included the *cdc24-m3* and *scp160KHΔ14* alleles. However, mutants in the negative regulators of mating exhibited similar MAPK pathway reporter expression as WT cells, but showed somewhat lower levels of shmoo formation. Thus, mutants in the negative regulators, which show enhanced mating (Figure 2D), do not show enhanced signaling or shmooing.

Quantitation of zygote formation

To assess whether the individual mutants show *bona fide* changes in chemotropism, we applied high-throughput imaging to mixed *MAT*a and *MAT*α cell populations. The method is based on the observation that the angle between two mating cells during zygote formation depends upon their precise orientation towards one another[46]. If their orientation (*i.e.* based upon gradient sensing) is optimal and cells grow directly towards one another, their angle of fusion is small and close to 0°. In contrast, an imperfect orientation to the pheromone gradient exhibits large fusion angles [46].

By using an ImageStream flow cytometer, we found that mutants of genes identified in the screen as positive regulators of mating demonstrate a profound defect upon gradient sensing (*i.e.* the average angle of orientation is ~40.3° (STD$\pm$4.3) for mutant (~134 cells of each mutant strain tested) crosses against WT cells versus ~12° (STD$\pm$1.03) for WT crosses against WT cells (152 cells tested) (Figure 4C). In contrast, the negative regulators of mating exhibited an improved orientation, being even slightly better than WT cells (*i.e.* the average angle of orientation is ~9.8° for mutants versus ~12° for WT cells).

Categorization of chemotropism mutants

Based upon the results from all of the various assays performed, we categorized the mutant strains according to their quantified similarity in phenotype, with respect to mating MAPK signaling, shmoo formation, and chemotropic growth. As mentioned above, many of the genes identified in the screen encode proteins with known functions connected to exocytosis and endocytosis, which regulate both pheromone receptor surface expression as well as the localization of polarity patches involved in gradient sensing and shmoo formation[9]. For convenience, we categorized the various gene hits into three groups.

Group I genes were characterized as being defective in both shmoo formation and chemotropism, however, they demonstrate optimal MAPK signaling. All of these genes (*e.g. YER008C/SEC3*,

YLR166C/SEC10, *YGL233W/SEC15*, and *YBR102C/EXO84*) functionally belong to the exocyst complex, which plays a critical role in vesicle tethering and secretion[47]. All, except *SEC3*, were isolated as DAmP alleles, given that exocyst components aside from Sec3 are essential. That exocytic factors were isolated as chemotropism mutants was not entirely unexpected, since shmoo orientation and development (*i.e.* growth along the axis of polarity) requires processes of the late secretory pathway (*i.e.* secretory vesicle transport, pheromone receptor delivery and recycling, polarity factor clustering, and polarized actin) and these proteins localize to the shmoo tip[48]. Thus, the Group I phenotype is likely due, in part, to pleiotropic effects caused by altered Ste2 pheromone receptor cycling and activation in these cells, as well as deficiencies in secretion, polarity factor/patch localization, and actin remodeling required for shmoo formation.

Group II genes (*e.g. TRS31, YPP1, BEM4, APS1, SFD1,* and *RAX1*) are defective in chemotropism (gradient sensing), with only a slight decrease or increase in signaling. These mutants demonstrate decreased ability to polarize growth during mating, but the cells still form shmoos. These genes encode for uncharacterized proteins (*SFD1*), proteins involved in cytoskeletal control/bud-shmoo site selection (*BEM4* and *RAX1*), and transport proteins involved in endocytosis and cycling of the Ste2 receptor (*TRS31, YPP1*, and *APS1*). Bem4 is a regulator of Cdc24 (and, thus, Cdc42 activation) and also interacts with the Ste11 MAPK in control of the mating signal[49]. Likewise, Rax1, which is involved in bud/shmoo site selection and whose deletion affects placement and angle of the mating projection, has been proposed to control Gpa1 and Cdc24 function[50]. Trs31 is a core component of the TRAPP vesicle tethering complex, which regulates traffic to and from the Golgi, but also facilitates post-Golgi vesicle trafficking[51]. Ypp1 is required for Stt4 phosphotidylinositol-4 kinase localization to the plasma membrane[52] and the clathrin-dependent endocytic internalization of Ste2 [53]. Aps1, a subunit of the clathrin AP-1 complex[54], likely functions in a similar capacity in Ste2 internalization.

Group III mutants (*e.g. SCP160*, *BUL3,* and *AHK1*) are defective in zygote orientation, signaling, and shmoo formation. While these three candidates share no known common functions between them, their mutants exhibit very similar, almost identical, phenotypes. *AHK1* encodes a putative scaffold component of the Hkr1 subbranch of the HOG signaling pathway and is required for transmission of the osmolarity stress response[55], as well as other signals via the Ste11 MAPK, which is required for mating. *BUL3* encodes a protein involved in the ubiquitin-mediated sorting of plasma membrane proteins associated with Rsp5 ubiquitin ligase activity[56], which mediates pheromone receptor internalization [57].

Arguably, Group I-III genes are likely involved in pheromone receptor transport and recycling and, thus, might be predictable in their defects in chemotropism and mating. However, **Group IV** genes (*e.g. YGR016W, SKA1, IRC19, GPR1, YML053C, IRA2,* and *ASC1*) are mutants that demonstrate optimal signaling, shmoo formation, and orientation, and show enhanced mating efficiency in ways that may be distinct from receptor recycling mechanisms. These genes comprise the negative regulators of chemotropism and appear to be involved in MAPK cascades. *GPR1* encodes the GPCR involved in glucose sensing involved in the filamentous growth pathway and acts upstream of adenylyl cyclase in a Ras-independent fashion[38, 39]. *IRA2* encodes a Ras-GTPase activating protein that lowers the activity of the Ras pathway and adenylyl cyclase[58]. *ASC1* encodes a ribosomal protein that acts downstream of the Gpr1 signaling to confer filamentous growth[13, 22, 25] and facilitates Scp160 association with polysomes[26]. Thus, three of the negative regulators of gradient sensing and chemotropism are directly involved in signaling along the filamentous growth pathway.

SKA1 encodes a protein proposed to facilitate exosome (3'-5' exonuclease) function in the catabolism of non-ribosome-associated mRNAs[59], while *YGR016W* encodes a protein of unknown function. While the connection of these proteins to the negative regulation of mating is unknown, both proteins were shown to be substrates of Rsp5[60]. Finally, *IRC19* has been suggested to function with other genes in restricting recombination events to regulate cell division[61], while *YML053C* encodes an uncharacterized protein also likely related to cell cycle control[62].

Deletion of *ASC1* enhances Scp160-mediated RNA binding and mating

The positive role of Gpa1-activated Scp160 in chemotropism and mating has been largely defined[19, 21], and is validated here (Figure 3B). However, we also identified Asc1 as a negative regulator of mating (Figure 2C and D). Asc1 is a ribosome-associated protein that facilitates Scp160 binding to polysomes[26] and acts as a downstream effector of Gpr1- and Gpa2-mediated filamentous growth[25]. This suggests that Scp160 and Asc1 functions are antagonistic to each other, and may illustrate how the two MAPK pathways intersect to regulate signal transduction at the level of translational control.

Since the RNA-binding function of Scp160 is specifically activated by pheromone signaling or constitutively active Gpa1 ($Gpa1^{Q323L}$)[21], we examined whether the deletion of *ASC1* has an effect upon the binding of mRNAs (Figure 5). We expressed FLAG epitope-tagged Scp160 from the genome along with either native or activated Gpa1 from single-copy plasmids in WT or *asc1Δ* cells. In these cells, we examined the binding of Scp160 to an mRNA (*FUS3*) known to bind upon

activation and another (*ASH1*) that does not[21]. As expected, the expression of Gpa1^{Q323L} enhanced *FUS3* (42-fold) but not *ASH1*, mRNA binding to FLAG-Scp160 in WT cells, whereas the expression of non-activated Gpa1 had no effect (Figure 5). Interestingly, the deletion of *ASC1* led to increased *FUS3* binding to FLAG-Scp160 in WT cells (either with or without the expression of native Gpa1), and strong enhancement (~200-fold binding) in cells expressing activated Gpa1 (Figure 5). Thus, Asc1 expression inhibits the RNA-binding function of Scp160, particularly in the absence of pheromone signaling.

Since the deletion of *ASC1* stimulates mating (Figure 2D), we determined whether the over-expression of *ASC1* in cells inhibits mating. We examined the mating efficiency of WT cells overexpressing *ASC1* from a multicopy plasmid, in comparison to WT cells alone or over-expressing *SCP160*, or to the *scp160Δ* and *asc1Δ* deletions (Figure S1). We found that the deletion of *ASC1* led to a 4.2-fold increase in mating efficiency, while its over-expression resulted a 24.4-fold decrease (Figure S1A). In contrast, the deletion of *SCP160* led to a 4.4-fold decrease in mating and its overexpression had almost no effect. Thus, both *ASC1* over-expression and deletion had robust effects on mating, whereas that of *SCP160* was more limited. Since *ASC1* has an intron, we also examined whether intron presence or removal had an effect on its ability to inhibit mating. However, both intronless and native *ASC1* had similar inhibitory effects (Figure S1B).

Scp160 sequesters Asc1 upon pheromone signaling

Given that Asc1 interacts with Scp160 [26] and acts as both an inhibitor of the mating pathway (Figure 2D) and modulator of the RNA-binding function of Scp160 (Figure 5), we examined whether its interaction with Scp160 is regulated via the Gpa1-mediated pheromone signaling pathway or the Gpa2-mediated filamentous growth signaling pathway (Figure 6). We expressed HA epitope-tagged Asc1 in WT cells or co-expressed either Gpa1^{Q323L} or activated Gpa2 (Gpa2^{Q355L}), and performed pulldowns using anti-HA antibodies. We observed that HA-Asc1 precipitated little Scp160 alone, but showed a large increase in Scp160 binding in the presence of added exogenous pheromone (α-factor) or Gpa1^{Q323L} (*i.e.* 4.4-fold and 3.5-fold, respectively) (Figure 6). In contrast, no Scp160 binding to Asc1 was observed in cells expressing Gpa2^{Q355L}. Thus, Scp160 binds to and sequesters Asc1 upon pheromone stimulation, but not during filamentous growth signaling.

***FUS3* mRNA granule formation and localization in pheromone-treated cells depends on both Scp160 and Asc1**

We previously demonstrated that *FUS3* mRNA localizes to the tip of the mating projection upon pheromone stimulation[21]. We examined the effect of either *SCP160* or *ASC1* deletion on *FUS3* mRNA granule formation and localization (Figure S2). Using MS2 aptamer-tagged *FUS3* expressed from the genome under its native promoter, we observed that whereas WT and *scp160Δ* cells had mostly single *FUS3* mRNA granules, *asc1Δ* cells had multiple granules in all cells scored (Figure S2A and B). This suggests that Asc1 has a role in the integrity of the *FUS3* granules. Moreover, we noted that the multiple *FUS3* mRNA granules observed in *asc1Δ* cells were not localized to the shmoo tip or body (*i.e.* near the tip), but instead were mislocalized throughout the cell body (Figure S2C). Likewise, the single mRNA granules observed in *scp160Δ* cells were also mislocalized (Figure S2C), thus, both Asc1 and Scp160 are required for the normal trafficking and localization of *FUS3* mRNA.

Fus3 expression and phosphorylation are not altered in cells lacking either *SCP160* or *ASC1*

Given that the deletion of either *ASC1* or *SCP160* affects the localization of Scp160 target mRNAs, like *FUS3*, we examined their effect on Fus3 protein expression and phosphorylation in response to pheromone signaling. We used anti-phospho ERK antibodies that recognize both Kss1-P (at 43kDa) and Fus3-P (at 41kDa) upon pheromone treatment[63] to detect the proteins in cell lysates (Figure S2D). We observed no differences in the levels of these phosphorylated MAPKs upon the deletion of either gene (Figure S2D). This indicates that pheromone signaling remains intact even though chemotropism and mating are strongly affected (Figures 2C and D, 3B, 4, and S1) and *FUS3* mRNA binding to Scp160 is altered in the absence of Asc1 (Figure 5). Thus, the effects exerted by the deletion of either gene are likely to be connected to altered mRNA localization and/or local translational control, in which both proteins participate.

Specific paralogs of ribosomal proteins control chemotropism

Given that Asc1 and Scp160 help control protein translation in cells, we re-examined the results of our initial screen (Figure 1B) for genes involved in translation (*e.g.* RPs) that had been removed from further analysis. By re-evaluating the role of these RPs in mating assays (after manual deletion), we identified specific RP paralogs involved in mating (*e.g. RPL9A*, *RPL12B*, *RPL19B, RPS21B,* and *RPS27B*) (Figure 7A). The deletions of *RPL12B* or *RPL19B*, but not *RPL12A* (Figure 7A) or *RPL19A*, were found to strongly inhibit mating, while those of *RPL9A*, *RPS21B,* and *RPS27B* increased mating (Figure 7A). Given that *RPL12B* and *RPL19B* encode positive regulators of mating, we subjected their deletion mutants to the pheromone confusion assay and found that neither

showed additional effects upon mating efficiency in the presence of exogenous α-factor (Figure 7B). Thus, Rpl12b and Rpl19b are indeed *bona fide* chemotropism mutants.

RP paralog specificity in pheromone signaling: *rpl12Δ* and *rpl19Δ* translatomes show reduced expression of proteins involved in mating

Recent work from our lab demonstrated that yeast lacking specific RP paralogs show large differences in their translatomes which incur changes in cell physiology[64]. This and other works suggest that RP paralog specificity in ribosomes is a defining element of translational control[65]. To examine the translatomes, we used PUNCH-P, which employs biotin-puromycin to label nascent polypeptides in isolated polysomes and mass spectrometry to identify translating proteins[64, 66].

Using cells manually deleted for the paralogs, we examined the translatomes of *rpl12aΔ* vs. *rpl12bΔ* cells and *rpl19aΔ* vs. *rpl19bΔ* cells in comparison to WT cells grown on glucose-containing medium, and looked for the effects on proteins related to mating according to gene ontology (GO) terms (Figure 8A). We were able to identify >700 proteins for each strain, of which the translation of many mating/cytoskeletal-related proteins was altered in a paralog-specific manner (Figure 8B and C). Proteins with reduced translation in *rpl12bΔ* cells (relative to *rpl12aΔ* cells) and *rpl19bΔ* cells (relative to *rpl19aΔ* cells) included specific mating components (*e.g.* Ste6, Far1, and Hbt1), as well as Scp160, and proteins involved in actin regulation and endocytosis (*e.g.* Twf1, Abp1, Sac6, Myo2, Myo5, and Rsp5)(Figure 8B and C). In contrast, we observed the upregulation of translation of other endocytic and actin-related proteins in *rpl12bΔ* and *rpl19bΔ* cells, such as Rvs167, Srv2, and Bem2 (Figure 8B and C). Thus, the changes in translational control observed in *rpl12bΔ* and *rpl19bΔ* cells (Figure 8) appear to correlate with changes in chemotropism and mating (Figure 7).

Discussion

The different MAPK cascades in yeast share conserved signaling modules containing kinases and scaffolding elements to generate intrinsic unidirectional signals that confer cellular responsiveness to a wide variety of extrinsic conditions (*e.g.* pheromone signaling, nutrient limitation, osmotic challenge, etc.)[67, 68]. Yet the properties that govern interplay between the signaling pathways leading to MAPK activation and readout are not fully understood. While studies have identified mutations that block mating as a consequence of defects in pheromone signaling and morphogenesis[69, 70], for example, no systematic attempt has been made to specifically identify regulators of chemotropism, a key feature of the cascade likely to be influenced by pathway cross-talk.

Here we have performed a systematic screen for positive and negative regulators of yeast mating, followed by secondary screening for mutants defective solely in gradient sensing and chemotropism (Figures 1 and 3, Table S2). Using this approach we validated 15 genes that when mutated inhibit chemotropic growth and subsequent mating (Figures 2A and B, 3B, 4 and 7), and 10 genes that act as negative regulators, as their mutation enhances mating (Figures 2C and D, 4, 7A, and S1). We initially classified these mutants into four different categories (Groups I-IV), depending upon their intrinsic levels of MAPK signaling, pheromone-induced morphogenesis, and angle of mating projection formation (a measure of gradient sensing) (Figure 4). Many of the regulators of chemotropism are known trafficking proteins involved in the delivery and retrieval of proteins to the cell surface, including the pheromone receptor, agglutinins, and pheromone. These include the Group I and II genes, along with *BUL3* (Group III), which are all strongly defective in mating when mutated (Figure 3). Based upon their roles in exocytosis and endocytosis, these genes might be expected to affect mating *per se* (via defects in general protein transport). However, their impact upon the angle of incidence between mating partners (Figure 4C) suggests they also intimately affect gradient sensing. Since pheromone signaling rearranges the spatial distribution of the Ste2 pheromone receptor from the entire cell surface to the shmoo tip[71], the Group I-III mutants likely impinge upon receptor cycling and, hence, local signaling. This may also involve localization of a mobile polarity site (or patch) that serves as a site of communication where pheromones are released and sensed[72, 73]. Patch dynamics (via the delivery of secretory vesicles, endocytic recycling and actin dynamics) are thought to continually correct its position and align it with the gradient from the mating partner through local pheromone sensing[9]. The transmission of downstream signals through the polarity patch may involve genes connected to the regulation of MAPK signaling, such as *BEM4* and *RAX1* (Group II), and *AHK1* (Group III),

identified in our screen (Figures 2A and B, and 3). These could potentiate patch dynamics, receptor signaling and cycling in part via phosphorylative control. Two of the Group IV genes, which are negative regulators of mating (Figure 2C and D), encode proteins that regulate the MAPK signaling module and buffer the pheromone signal. These include Gpr1 and Gpa2, which are the receptor and Gα for the nutrient sensing (filamentous growth) pathway, respectively[23, 24, 38, 39], and compete with the pheromone receptors (Ste2 or Ste3) and Gpa1 for signaling via the Ste20-Ste11-Ste7 kinase cascade that activates the Kss1 MAPK, instead of Fus3[40]. Thus, the inactivation of these genes potentiates the mating pathway, similar to the deletion of *IRA2* (also Group IV), which is a negative regulator of the RAS pathway that activates adenylyl cyclase and the nutrient sensing pathway[74]. Finally, we identified RPs as specific regulators of the mating pathway, including positive (chemotropic growth) regulators, such as Asc1, Rpl12b and Rpl19b (Group IV), and negative regulators such as Rpl9a, Rps21b, and Rps27b (Figure 7), which are involved in translational control. Thus, our screen essentially identified three sets of genes involved in: 1) protein trafficking; 2) MAPK signal transduction; and 3) translational control, as regulators of chemotropic growth and subsequent mating. We note that it is likely that additional genes relevant to these processes were missed in our screen due to absence in the library, as a consequence of their impact upon mating during library preparation. Correspondingly, some DAmP library alleles may not yield a phenotype sufficiently robust to result in detectable defects in mating. And finally, our bias to remove genes associated with translation, mitochondrial function, and metabolism may have resulted in missed genes, as evidenced *post facto* (Figures 7 and 8).

As proteins involved in trafficking and signaling were obvious candidates for regulatory elements, we were surprised to identify RPs as both negative (*e.g.* Asc1, Rpl9a, Rps21b, and Rps27b) and positive regulators (*e.g.* Rpl12b, and Rpl19b), although we knew that Scp160 has a role in translational control[75]. Importantly, we identified a tight genetic and physical interaction between Asc1 and Scp160 that likely explains their opposing effects on the mating and filamentous growth pathways. We found that the deletion of *ASC1*, which is required for filamentous growth[25], led to large enhancement in mating efficiency, while its over-expression had the opposite effect (Figure S1). Moreover, Scp160 binds Asc1 upon pheromone stimulation or Gpa1 activation, but not upon Gpa2 activation (Figure 6). Thus, the mating and filamentous growth MAPK pathways intersect at the level of Scp160 and Asc1, whereby pheromone/Gpa1-activated Scp160 mediates Asc1 binding to control readout of the two pathways at the level of translational control (Figure S3). Productive Scp160-Asc1 interactions, which have been shown to enhance translation on polysomes[26], lead to propagation of the mating signal and, as a

consequence, inhibition of the nutrient sensing/filamentous growth signals.

We also were surprised to see RPs as direct regulators of chemotropism and mating, which lends credence to the idea that incumbent with Gβγ activation of Ste20 and downstream signaling, Gα signals lead to changes in translational control of proteins connected directly to the mating pathway. This is borne out by experiments showing that the translatomes of *rpl12b*Δ and *rpl19b*Δ cells are deficient in proteins required for mating, as compared to WT, *rpl12a*Δ and *rpl19a*Δ cells (Figure 8). Thus, a translational control pathway involving Scp160 and specific RP paralogs plays a major role in propagation of the mating signal. Likewise, we expect that Asc1 and yeast RP paralogs: Rpl9a, Rps21b, and Rps27b, confer translational control of proteins involved in propagation of filamentous growth pathway signals. Thus, we have identified translational control as a direct means to modulate signals conferred by different MAPK cascades to control cellular responsiveness to extracellular signals. Moreover, we further extend our knowledge of RP paralog specificity, in terms of its direct involvement in translation and control of cell physiology[65, 76].

Since gradient sensing and chemotropism/chemotaxis are highly relevant to the growth and migration of mammalian cells in complex microenvironments[77, 78], there are likely to be structural and functional similarities to those underlying the yeast chemotropic response. Thus, some of the genes identified here may act as homologous regulators participate in these processes. For example, mammalian Asc1 (RACK1) was earlier shown to regulate cell migration via its interaction with Gβ/γ and its downregulation enhances chemotaxis[79]. Numerous later studies reveal that this RP interacts with a wide variety of receptors and receptor-mediated signaling pathways to shuttle interacting partners, modify their activity, regulate their associations, and modulate stability[80]. Thus, Asc1/RACK1 is a prime candidate for MAPK pathway go-between to regulate chemotropic/chemotaxic responses to external signals. Whether its connection to mammalian Scp160 (vigilin)[81] has been maintained in evolution remains unknown. Likewise, no study has examined the role of vigilin in either chemotropism or chemotaxis. Yet, our demonstration of Scp160 binding of Asc1 upon Gpa1 Gα activation to downregulate its functions will prompt us in the future to determine the outcome upon cellular translation, and may prompt others to study their possible connection in higher organisms.

Acknowledgements

The authors are grateful to Ralf Jansen (U. Tuebingen, Germany) for the gift of anti-Scp160 antibodies and to Pnina Weissman and Silvia Chuarzman for help with the screen in yeast. R.G-L. was supported in part by a returning scientist fellowship from the Israel Ministry of Absorption. This work was supported in part by an internal grants from the Jeanne and Joseph Nissim Center for Life Sciences Research and the Vice President's Dedicated Equipment Fund, Weizmann Institute of Science. J.E.G. holds the Besen-Brender Chair in Microbiology and Parasitology, Weizmann Institute of Science. M.S is an incumbent of the Dr. Gilbert Omenn and Martha Darling Professorial Chair in Molecular Genetics. A.L., P.C. and R. G.-L. were supported in part by NIH grants GM084332 and CA209992.

Methods

Yeast Strains

Yeast strains used in this study are listed in Table S2.

Mating efficiency screens:

Automated library preparation

A SGA-ready *MAT*α wild-type strain bearing the *TEF2pr-mCherry* gene integrated into the HO locus was crossed against yeast deletion[34] and DAmP[35] libraries using the SGA method[82, 83]) A RoToR bench-top colony array instrument (pinning robot; Singer Instruments, Somerset UK) was used to pin the libraries. Strains from opposing mating types harboring the desired genomic manipulations (*i.e.* the mutation/deletion libraries on the one hand and the cytosolic mCherry WT strain on the other) were crossed and diploid cells selected on selective medium. Sporulation was induced by transferring yeast to nitrogen starvation media for 7 days, following which specific haploid progeny of *MAT*a were selected by growth on medium lacking histidine and using both canavanine and thia-lysine selection (Sigma-Aldrich) to select against remaining diploids. The resultant libraries contained the desired genotypes. Representative strains of the resulting yeast libraries were verified by PCR.

Mating efficiency and confusion screens

The query strain (*MAT*α wild-type) expressing *TEF2pr-GFP*, as well as the *MAT*a gene knockout and attenuated (DAmP) libraries (384-well plates) were inoculated and grown in liquid YPD overnight at 30°C. Subsequently, cells were diluted and grown (4-5hrs) until reaching mid-log phase. Both the libraries and query strain were then plated by pinning (1.5mm diameter) onto separate YPD agar plates and grown overnight at 30°C. Following which, the *MAT*α query strain and library plates were pinned together onto fresh YPD plates and allowed to grow for 4hrs at 30°C for mating. The individual *MAT*α–*MAT*a crosses were then pinned into 1xTE in concanavalin-A coated 384-well glass bottom plates, centrifuged briefly to precipitate the cells, fixed using 4% paraformaldehyde (15min), and then washed twice with phosphate-sorbitol buffer (0.1M potassium phosphate pH7.5, 1.2M sorbitol). For the confusion assay, the *MAT*α–*MAT*a crosses were plated onto fresh YPD agar plates containing 30μM α-factor (Sigma-Aldrich) and allowed to grow for 4hrs at 30°C prior to fixation.

High-throughput microscopy

Crosses from the mating efficiency screen were visualized at room temperature using an automated inverted fluorescence microscopic ScanR system (Olympus Corp., Tokyo Japan). Images were acquired using a 60× air objective (NA 0.9) with excitation at 490/20 nm (GFP) or 572/35 nm (RFP) and with an ORCA-ER charge-coupled device camera (Hamamatsu). After acquisition, images were manually reviewed using the ImageJ analysis program.

IP and RNA binding

The immunoprecipitation of protein-RNA complexes was as described in Gelin-Licht *et al.* [21]. Briefly, yeast cells expressing FLAG-tagged Scp160 were grown on synthetic medium to mid-log phase, lysed in lysis buffer (20mM Tris-Cl, pH 7.5, 150mM KCl, 5mM $MgCl_2$, 100U/ml RNasin [Promega, Madison, WI, USA], 0.1% NP-40, protease inhibitor cocktail), and broken by vortexing with glass beads. For each anti-FLAG immunoprecipitation (IP) 4mg of the TCL was diluted in lysis buffer (final volume, 0.5ml), subjected to IP with anti-FLAG M2 affinity gel (30µl; Sigma, St. Louis, MO, USA) overnight at 4°C with rotation. The precipitates were then washed (x5) with lysis buffer. The precipitated protein-RNA complexes were eluted by incubation in 300µl of elution buffer, containing 50mM Tris-HCl, pH8.0, 100mM NaCl, 10mM EDTA, 0.1% SDS with 100µg/µl proteinase K (Promega, Madison, WI, USA), at 65°C for 30min.

RNA was purified from the IP eluates using the Masterpure™ Yeast RNA purification kit (Epicenter, Madison, USA), according to the manufacturer's instructions. After precipitation with added glycogen (8µg/ml; Roche, Mannheim, Germany) and 0.3M sodium acetate (pH5.0), the RNA was resuspended in 30µl of diethyl pyrocarbonate-treated water, treated with 3 units/sample of DNase I for 2 hours (Promega, Madison, WI, USA), and 1-3µl aliquots were taken for reverse transcription (RT) using the Moloney murine leukemia virus RT RNase H (−) (Promega, Madison, WI, USA), according to the manufacturer's instructions, to yield cDNA. In parallel, total cellular RNA was purified from 15µl of TCL using the Masterpure™ Yeast RNA purification kit, treated with DNase I, and 1-2µg of RNA was taken for RT, in the same manner as described above to yield total cDNA.

Real-time PCR was performed using the LightCycler 480 SYBR Green and LightCycler 480 system (Roche Diagnostics, Mannheim, Germany), according to the manufacturer's instructions. Reaction mixtures (10µl final volume) contained the following components: 3µl of cDNA, 5pmol forward and reverse primers, and LightCycler 480 SYBR Green PCR Master mix, as prescribed by the manufacturer. The primer pairs for *FUS3* and *ASH1* produced only one amplicon when tested by conventional RT-PCR. The levels of specific mRNAs in the different strains tested were assessed

relative to those obtained from precipitates derived from untreated (*i.e.* without pheromone or the expression of activated Gpa1) cells expressing FLAG-Scp160. The levels of specific mRNAs obtained from the different IP samples were normalized according to those of the total RNA.

Co-Immunoprecipitation

The immunoprecipitation of protein-protein complexes was as described in Gelin-Licht *et al.* [21]. Briefly, WT (BY4741) cells, WT cells expressing HA-tagged *ASC1* treated with or without α-factor, or HA-tagged *ASC1* cells co-expressing either $GPA1^{Q323L}$ or $GPA2^{Q355L}$ were grown to mid-log phase ($O.D._{600}$ = ~0.5) in 200ml synthetic selective medium at 26°C. Cultures were centrifuged at 3,000 x *g* for 5min at 4°C and resuspended in 1ml of lysis buffer (20mM Tris-Cl pH 7.5, 150mM KCl, 5mM MgCl2, 100U/ml RNasin, 0.1% NP-40, 1mM dithiothreitol, 2µg/ml aprotinin, 1µg/ml pepstatin, 0.5µg/ml leupeptin, and 0.01µg/ml benzamidine). Cells (100 $O.D._{600}$ units each) were broken by vortexing with glass beads (0.5mm size) for 10min at 4°C and centrifuged at 10,000 × *g* for 10 min at 4°C to yield the total cell lysate (TCL). For IP, 0.5mg of TCL was diluted in lysis buffer (final volume, 1 ml) and subjected to IP with monoclonal anti-HA-Agarose antibody (A2095; Sigma) overnight at 4°C with rotation. Next, the precipitates were washed (×5) with lysis buffer and protein–protein complexes were eluted by incubation at 100°C for 5 min with an appropriate volume of 5X protein sample buffer (5X: 0.4 M Tris at pH 6.8, 50% glycerol, 10% SDS, 0.5 M DTT, and 0.25% bromophenol blue).

For Western analysis, samples were electrophoresed on 10% SDS-PAGE gels. Protein detection using anti-HA (H9658, Sigma) or anti-Scp160 antibodies (Gift of R. Jansen, U. Tuebingen) was performed using the Amersham ECL Western Blotting Detection Kit (GE Healthcare Life Sciences). Quantification of protein bands was performed using ImageJ software.

Quantitative Mating Assay

The quantitative mating assay was performed as described previously[84]. The assay is based on the complementation of auxotrophic markers present in *MAT*a and *MAT*α cells upon crossing (*i.e. met15* mutation in *MAT*a BY4741 cells and *lys2* mutation in *MAT*α BY4742 cells are rescued upon mating to yield a diploid capable of growing on medium lacking methionine or lysine). Cultures were grown to an OD_{600} = 0.3-0.4 at 26°C and 10^6 cells of each strain (in a volume of ~150µl), as well as *MAT*a and *MAT*α mixtures, were collected by filtration on individual cellulose nitrate disk filters (25mm diameter, 0.45µm pore filters; BA-85 Schleicher & Schuell, Maidstone, UK) placed on top of the working filtration surface of a 500ml filtration apparatus (Corning, NY, USA). After

filtration, each filter was placed cell-side up on YPD plates for 90min at 30°C, before resuspension in 1ml of SC-Met/-Lys (or SC-Trp/-Lys) in a sterile 15ml tube, followed by vortexing, serial dilution (1:10,100,1000), and plating 100μl of the dilutions onto SC-Met/-Lys (or SC-Trp/-Lys) plates to select for diploids. Mating efficiency was determined by colony counting after 3 days at 26°C.

Quantitative analysis of angle of zygote formation

Mutant and wild-type strains of mating type A, expressing mCherry from TEF2 promotor and wild type strain of mating type alpha, expressing GFP from TEF2 promotor were grown in YPD to mid-log phase. Equal numbers ($1x10^6$) of *MAT*a and *MAT*α were mixed and collected by filtration on individual cellulose nitrate filters (e.g. 25mm diameter, 0.45μm pore filters; BA-85 Schleicher & Schuell, Maidstone, UK) placed on top of the working filtration surface of a 500ml filtration apparatus (Corning, NY, USA). After filtration the cells were removed from the filters to TE medium and fixed with 4% paraformaldehyde.

Cells were imaged by an Imaging Flow Cytometer (ImageStreamX Mark II, AMNIS-Luminex, Austin TX, USA). Data was acquired using a 60X lens, and lasers used were 488nm (100mW), 561nm (200mW), and 785nm (5mW). Data was analyzed using the manufacturer's software IDEAS 6.2 (AMNIS corp.). Images were compensated for spectral ovelap using single stained controls. Cells were first gated according to their area (in μm^2) and aspect ratio (the Minor Axis divided by the Major Axis of the best-fit ellipse). Cells were further gated for focus using the Gradient RMS and contrast features (that measure the sharpness quality of an image by detecting large changes of pixel values in the image). Only objects with positive signals for both GFP and mCherry were gated, using single stained cells as controls. To identify the relevant cell interactions, two additional features were used: lobe count (that counts the lobes within an object) and Symmetry 3 (that measures the tendency of the object to have a three-fold axis of symmetry). To calculate the overlap between the GFP and mCherry, a similarity feature was used to measure the degree of which two images are linearly correlated, and was calculated as log transformed Pearson's Correlation Coefficient.

PUNCH-P:

Nascent peptide Isolation

Nascent peptide Isolation and mass spectrometry for yeast were performed as previously described[64]. Briefly, 500 ml of yeast strains were grown in YPD at 30°C till mid-log phase ($O.D._{600}$ = 0.6–0.8). Cells were washed once with ice-cold double-distilled water, snap-frozen, and stored at -

80°C. Frozen yeast cells were suspended in polysome extraction buffer (PEB; 20 mM Tris-HCl, pH 7.4, 140 mM KCl, 10 mM MgCl2, 0.5 mM DTT, 2 µg/ml leupeptin, 40 U/ml RNAsin, 1.4 µg/ml pepstatin, 0.2 mg/ml heparin [Sigma-Aldrich], EDTA-free complete protease inhibitor mix [Roche], and 1% Triton X-100) and lysed using glass beads (0.4–0.6 mm).The lysates were centrifuged at 17,400 x *g* for 30 min at 4°C to remove cell debris. Following this, 6ml of supernatant was loaded on a 2.5 ml 70% sucrose cushion. The samples were centrifuged at 60,000 rpm at 4°C for 2hr in an SW65 Ti ultracentrifuge rotor (Beckman Coulter, California, USA). The translucent polysome pellets were washed by gently dispensing and removing 500 µl of ice-cold RNase-free water. Ribosomes were suspended in 150 µl PEB (without detergent) snap-frozen and stored at -80°C. Purification of nascent polypeptide chains by Biotin-dc-puromycin labeling and pulldown using streptavidin beads was performed as described previous protocols[85]. For each sample, 12 $O.D._{254}$ U of polysomes were incubated with 100 pmol of biotin-dc-puromycin (Jena Bioscience, Germany) per $O.D._{254}$ unit at 37°C for 15 min. For each sample, 5 µl of streptavidin beads (GE Healthcare, Chicago, USA) per $O.D._{254}$ unit was added, supplemented with 1 ml of SDS–urea buffer (50 mM Tris-HCl, pH 7.5, 8 M urea, 2% [wt/vol] SDS, and 200 mM NaCl), and incubated overnight at RT. The beads were washed five times with 1 ml SDS–urea buffer and incubated in 1 M NaCl for 30 min at 23°C followed by five washes in Ultrapure water.

Digestion and liquid chromatography mass spectrometry

The samples were subjected to on-bead tryptic digestion in the presence of urea. The resulting peptides were analyzed using nanoflow liquid chromatography (nanoAcquity; Waters Corp., Milford MA, USA) coupled to high resolution, high mass accuracy mass spectrometry. Each sample was analyzed on the instrument separately in a random order in discovery mode.

Data processing

Raw data was processed with MaxQuant v1.6.0.16. The data were searched using the Andromeda search engine against the *Saccharomyces cerevisiae* (strain S288c) proteome database appended with common lab protein contaminants and the following modifications: *e.g.* fixed modification - cysteine carbamidomethylation; variable modifications - methionine oxidation, asparagine and glutamine deamidation, and protein N-terminal acetylation. A total of 952 proteins were identified.

Mating-related proteins were shorted by looking at the functional annotation of all identified proteins using DAVID[86]. We identified 34 out of 952 detected proteins as mating-related and used their translatome data for further analysis.

Differential protein expression analysis

Protein quantification was performed using the Differential Enrichment analysis of Proteomics data (DEP) package of R software (https://doi.org/doi:10.18129/B9.bioc.DEP). Two out of three biological replicates for each condition were selected for differential protein expression analysis. The intensity values were log-transformed and only proteins that had valid values in at least one experimental group were kept. Missing values were imputed (*i.e.* replacing missing values by a normal distribution of low values) [87]. Finally, clustering (hierarchical) for each strain and volcano plots of one paralog vs. the other were performed using the same package.

References

1. Badisco, L., Van Wielendaele, P. & Vanden Broeck, J. Eat to reproduce: a key role for the insulin signaling pathway in adult insects. *Front Physiol* **4**, 202 (2013).
2. John, D. & Berg, D.K. Long-lasting changes in neural networks to compensate for altered nicotinic input. *Biochem Pharmacol* **97**, 418-424 (2015).
3. Pak, E. & Segal, R.A. Hedgehog Signal Transduction: Key Players, Oncogenic Drivers, and Cancer Therapy. *Dev Cell* **38**, 333-344 (2016).
4. Sudhof, T.C. Synaptic Neurexin Complexes: A Molecular Code for the Logic of Neural Circuits. *Cell* **171**, 745-769 (2017).
5. Gulei, D. *et al.* The "good-cop bad-cop" TGF-beta role in breast cancer modulated by non-coding RNAs. *Biochim Biophys Acta Gen Subj* **1861**, 1661-1675 (2017).
6. Collins, K.D., Lacal, J. & Ottemann, K.M. Internal sense of direction: sensing and signaling from cytoplasmic chemoreceptors. *Microbiol Mol Biol Rev* **78**, 672-684 (2014).
7. Lin, B. & Levchenko, A. Spatial manipulation with microfluidics. *Front Bioeng Biotechnol* **3**, 39 (2015).
8. Ismael, A. & Stone, D.E. Yeast chemotropism: A paradigm shift in chemical gradient sensing. *Cell Logist* **7**, e1314237 (2017).
9. Martin, S.G. Molecular mechanisms of chemotropism and cell fusion in unicellular fungi. *J Cell Sci* **132** (2019).
10. Swaney, K.F., Huang, C.H. & Devreotes, P.N. Eukaryotic chemotaxis: a network of signaling pathways controls motility, directional sensing, and polarity. *Annu Rev Biophys* **39**, 265-289 (2010).
11. Roca-Cusachs, P., Sunyer, R. & Trepat, X. Mechanical guidance of cell migration: lessons from chemotaxis. *Curr Opin Cell Biol* **25**, 543-549 (2013).
12. Thomas, M.A., Kleist, A.B. & Volkman, B.F. Decoding the chemotactic signal. *J Leukoc Biol* **104**, 359-374 (2018).
13. DeWire, S.M., Ahn, S., Lefkowitz, R.J. & Shenoy, S.K. Beta-arrestins and cell signaling. *Annu Rev Physiol* **69**, 483-510 (2007).
14. Paliwal, S. *et al.* MAPK-mediated bimodal gene expression and adaptive gradient sensing in yeast. *Nature* **446**, 46-51 (2007).
15. Jin, T. Gradient sensing during chemotaxis. *Curr Opin Cell Biol* **25**, 532-537 (2013).
16. Arkowitz, R.A. Chemical gradients and chemotropism in yeast. *Cold Spring Harb Perspect Biol* **1**, a001958 (2009).
17. Bardwell, L. A walk-through of the yeast mating pheromone response pathway. *Peptides* **26**, 339-350 (2005).
18. Dohlman, H.G. G proteins and pheromone signaling. *Annu Rev Physiol* **64**, 129-152 (2002).
19. Guo, M. *et al.* The yeast G protein alpha subunit Gpa1 transmits a signal through an RNA binding effector protein Scp160. *Mol Cell* **12**, 517-524 (2003).
20. Lang, B.D. & Fridovich-Keil, J.L. Scp160p, a multiple KH-domain protein, is a component of mRNP complexes in yeast. *Nucleic Acids Res* **28**, 1576-1584 (2000).
21. Gelin-Licht, R., Paliwal, S., Conlon, P., Levchenko, A. & Gerst, J.E. Scp160-dependent mRNA trafficking mediates pheromone gradient sensing and chemotropism in yeast. *Cell Rep* **1**, 483-494 (2012).
22. Gallo, S. & Manfrini, N. Working hard at the nexus between cell signaling and the ribosomal machinery: An insight into the roles of RACK1 in translational regulation. *Translation (Austin)* **3**, e1120382 (2015).
23. Kubler, E., Mosch, H.U., Rupp, S. & Lisanti, M.P. Gpa2p, a G-protein alpha-subunit, regulates growth and pseudohyphal development in Saccharomyces cerevisiae via a cAMP-dependent mechanism. *J Biol Chem* **272**, 20321-20323 (1997).

24. Lorenz, M.C. & Heitman, J. Yeast pseudohyphal growth is regulated by GPA2, a G protein alpha homolog. *EMBO J* **16**, 7008-7018 (1997).
25. Zeller, C.E., Parnell, S.C. & Dohlman, H.G. The RACK1 ortholog Asc1 functions as a G-protein beta subunit coupled to glucose responsiveness in yeast. *J Biol Chem* **282**, 25168-25176 (2007).
26. Baum, S., Bittins, M., Frey, S. & Seedorf, M. Asc1p, a WD40-domain containing adaptor protein, is required for the interaction of the RNA-binding protein Scp160p with polysomes. *Biochem J* **380**, 823-830 (2004).
27. Kouba, T., Rutkai, E., Karaskova, M. & Valasek, L. The eIF3c/NIP1 PCI domain interacts with RNA and RACK1/ASC1 and promotes assembly of translation preinitiation complexes. *Nucleic Acids Res* **40**, 2683-2699 (2012).
28. Opitz, N. *et al.* Capturing the Asc1p/Receptor for Activated C Kinase 1 (RACK1) Microenvironment at the Head Region of the 40S Ribosome with Quantitative BioID in Yeast. *Mol Cell Proteomics* **16**, 2199-2218 (2017).
29. Gerbasi, V.R. *et al.* Critical Role for Saccharomyces cerevisiae Asc1p in Translational Initiation at Elevated Temperatures. *Proteomics* **18**, e1800208 (2018).
30. Segall, J.E. Polarization of yeast cells in spatial gradients of alpha mating factor. *Proc Natl Acad Sci U S A* **90**, 8332-8336 (1993).
31. Hagen, D.C., McCaffrey, G. & Sprague, G.F., Jr. Pheromone response elements are necessary and sufficient for basal and pheromone-induced transcription of the FUS1 gene of Saccharomyces cerevisiae. *Mol Cell Biol* **11**, 2952-2961 (1991).
32. Barale, S., McCusker, D. & Arkowitz, R.A. Cdc42p GDP/GTP cycling is necessary for efficient cell fusion during yeast mating. *Mol Biol Cell* **17**, 2824-2838 (2006).
33. Kuzmin, E., Costanzo, M., Andrews, B. & Boone, C. Synthetic Genetic Arrays: Automation of Yeast Genetics. *Cold Spring Harb Protoc* **2016**, pdb top086652 (2016).
34. Giaever, G. *et al.* Functional profiling of the Saccharomyces cerevisiae genome. *Nature* **418**, 387-391 (2002).
35. Breslow, D.K. *et al.* A comprehensive strategy enabling high-resolution functional analysis of the yeast genome. *Nat Methods* **5**, 711-718 (2008).
36. Liu, J. & Guo, W. The exocyst complex in exocytosis and cell migration. *Protoplasma* **249**, 587-597 (2012).
37. Peng, Y. *et al.* Regulation of dendrite growth and maintenance by exocytosis. *J Cell Sci* **128**, 4279-4292 (2015).
38. Xue, Y., Batlle, M. & Hirsch, J.P. GPR1 encodes a putative G protein-coupled receptor that associates with the Gpa2p Galpha subunit and functions in a Ras-independent pathway. *EMBO J* **17**, 1996-2007 (1998).
39. Kraakman, L. *et al.* A Saccharomyces cerevisiae G-protein coupled receptor, Gpr1, is specifically required for glucose activation of the cAMP pathway during the transition to growth on glucose. *Mol Microbiol* **32**, 1002-1012 (1999).
40. Madhani, H.D. & Fink, G.R. The riddle of MAP kinase signaling specificity. *Trends Genet* **14**, 151-155 (1998).
41. Belli, G., Gari, E., Piedrafita, L., Aldea, M. & Herrero, E. An activator/repressor dual system allows tight tetracycline-regulated gene expression in budding yeast. *Nucleic Acids Res* **26**, 942-947 (1998).
42. Nern, A. & Arkowitz, R.A. A GTP-exchange factor required for cell orientation. *Nature* **391**, 195-198 (1998).
43. Dorer, R., Pryciak, P.M. & Hartwell, L.H. Saccharomyces cerevisiae cells execute a default pathway to select a mate in the absence of pheromone gradients. *J Cell Biol* **131**, 845-861 (1995).

44. Li, A.M. *et al.* Both KH and non-KH domain sequences are required for polyribosome association of Scp160p in yeast. *Nucleic Acids Res* **32**, 4768-4775 (2004).
45. Bagnat, M. & Simons, K. Cell surface polarization during yeast mating. *Proc Natl Acad Sci U S A* **99**, 14183-14188 (2002).
46. Stone, D.E. & Arkowitz, R.A. In Situ Assays of Chemotropism During Yeast Mating. *Methods Mol Biol* **1407**, 1-12 (2016).
47. Lepore, D.M., Martinez-Nunez, L. & Munson, M. Exposing the Elusive Exocyst Structure. *Trends Biochem Sci* **43**, 714-725 (2018).
48. Narayanaswamy, R. *et al.* Systematic definition of protein constituents along the major polarization axis reveals an adaptive reuse of the polarization machinery in pheromone-treated budding yeast. *J Proteome Res* **8**, 6-19 (2009).
49. Pitoniak, A. *et al.* Cdc42p-interacting protein Bem4p regulates the filamentous-growth mitogen-activated protein kinase pathway. *Mol Cell Biol* **35**, 417-436 (2015).
50. Vasen, G., Dunayevich, P. & Colman-Lerner, A. Mitotic and pheromone-specific intrinsic polarization cues interfere with gradient sensing in Saccharomyces cerevisiae. *Proc Natl Acad Sci U S A* **117**, 6580-6589 (2020).
51. Lipatova, Z. & Segev, N. Ypt/Rab GTPases and their TRAPP GEFs at the Golgi. *FEBS Lett* **593**, 2488-2500 (2019).
52. Baird, D., Stefan, C., Audhya, A., Weys, S. & Emr, S.D. Assembly of the PtdIns 4-kinase Stt4 complex at the plasma membrane requires Ypp1 and Efr3. *J Cell Biol* **183**, 1061-1074 (2008).
53. Yamamoto, W. *et al.* Distinct roles for plasma membrane PtdIns(4)P and PtdIns(4,5)P2 during receptor-mediated endocytosis in yeast. *J Cell Sci* **131** (2018).
54. Phan, H.L. *et al.* The Saccharomyces cerevisiae APS1 gene encodes a homolog of the small subunit of the mammalian clathrin AP-1 complex: evidence for functional interaction with clathrin at the Golgi complex. *EMBO J* **13**, 1706-1717 (1994).
55. Nishimura, A. *et al.* Scaffold Protein Ahk1, Which Associates with Hkr1, Sho1, Ste11, and Pbs2, Inhibits Cross Talk Signaling from the Hkr1 Osmosensor to the Kss1 Mitogen-Activated Protein Kinase. *Mol Cell Biol* **36**, 1109-1123 (2016).
56. Novoselova, T.V., Zahira, K., Rose, R.S. & Sullivan, J.A. Bul proteins, a nonredundant, antagonistic family of ubiquitin ligase regulatory proteins. *Eukaryot Cell* **11**, 463-470 (2012).
57. Dunn, R. & Hicke, L. Domains of the Rsp5 ubiquitin-protein ligase required for receptor-mediated and fluid-phase endocytosis. *Mol Biol Cell* **12**, 421-435 (2001).
58. Tanaka, K. *et al.* IRA2, a second gene of Saccharomyces cerevisiae that encodes a protein with a domain homologous to mammalian ras GTPase-activating protein. *Mol Cell Biol* **10**, 4303-4313 (1990).
59. Zhang, E. *et al.* A specialised SKI complex assists the cytoplasmic RNA exosome in the absence of direct association with ribosomes. *EMBO J* **38**, e100640 (2019).
60. Gupta, R. *et al.* Ubiquitination screen using protein microarrays for comprehensive identification of Rsp5 substrates in yeast. *Mol Syst Biol* **3**, 116 (2007).
61. Alvaro, D., Lisby, M. & Rothstein, R. Genome-wide analysis of Rad52 foci reveals diverse mechanisms impacting recombination. *PLoS Genet* **3**, e228 (2007).
62. Niu, W., Li, Z., Zhan, W., Iyer, V.R. & Marcotte, E.M. Mechanisms of cell cycle control revealed by a systematic and quantitative overexpression screen in S. cerevisiae. *PLoS Genet* **4**, e1000120 (2008).
63. Cullen, P.J. Evaluating the activity of the filamentous growth mitogen-activated protein kinase pathway in yeast. *Cold Spring Harb Protoc* **2015**, 276-283 (2015).
64. Segev, N. & Gerst, J.E. Specialized ribosomes and specific ribosomal protein paralogs control translation of mitochondrial proteins. *J Cell Biol* **217**, 117-126 (2018).

65. Gerst, J.E. Pimp My Ribosome: Ribosomal Protein Paralogs Specify Translational Control. *Trends Genet* **34**, 832-845 (2018).
66. Aviner, R., Geiger, T. & Elroy-Stein, O. Novel proteomic approach (PUNCH-P) reveals cell cycle-specific fluctuations in mRNA translation. *Genes Dev* **27**, 1834-1844 (2013).
67. Raman, M., Chen, W. & Cobb, M.H. Differential regulation and properties of MAPKs. *Oncogene* **26**, 3100-3112 (2007).
68. Chen, R.E. & Thorner, J. Function and regulation in MAPK signaling pathways: lessons learned from the yeast Saccharomyces cerevisiae. *Biochim Biophys Acta* **1773**, 1311-1340 (2007).
69. Hartwell, L.H. Mutants of Saccharomyces cerevisiae unresponsive to cell division control by polypeptide mating hormone. *J Cell Biol* **85**, 811-822 (1980).
70. Narayanaswamy, R. *et al.* Systematic profiling of cellular phenotypes with spotted cell microarrays reveals mating-pheromone response genes. *Genome Biol* **7**, R6 (2006).
71. Emmerstorfer-Augustin, A., Augustin, C.M., Shams, S. & Thorner, J. Tracking yeast pheromone receptor Ste2 endocytosis using fluorogen-activating protein tagging. *Mol Biol Cell* **29**, 2720-2736 (2018).
72. Dyer, J.M. *et al.* Tracking shallow chemical gradients by actin-driven wandering of the polarization site. *Curr Biol* **23**, 32-41 (2013).
73. Merlini, L. *et al.* Local Pheromone Release from Dynamic Polarity Sites Underlies Cell-Cell Pairing during Yeast Mating. *Curr Biol* **26**, 1117-1125 (2016).
74. Conrad, M. *et al.* Nutrient sensing and signaling in the yeast Saccharomyces cerevisiae. *FEMS Microbiol Rev* **38**, 254-299 (2014).
75. Hirschmann, W.D. *et al.* Scp160p is required for translational efficiency of codon-optimized mRNAs in yeast. *Nucleic Acids Res* **42**, 4043-4055 (2014).
76. Genuth, N.R. & Barna, M. Heterogeneity and specialized functions of translation machinery: from genes to organisms. *Nat Rev Genet* **19**, 431-452 (2018).
77. Roussos, E.T., Condeelis, J.S. & Patsialou, A. Chemotaxis in cancer. *Nat Rev Cancer* **11**, 573-587 (2011).
78. Suter, T. & Jaworski, A. Cell migration and axon guidance at the border between central and peripheral nervous system. *Science* **365** (2019).
79. Chen, S. *et al.* RACK1 regulates directional cell migration by acting on G betagamma at the interface with its effectors PLC beta and PI3K gamma. *Mol Biol Cell* **19**, 3909-3922 (2008).
80. Li, J.J. & Xie, D. RACK1, a versatile hub in cancer. *Oncogene* **34**, 1890-1898 (2015).
81. Cheng, M.H. & Jansen, R.P. A jack of all trades: the RNA-binding protein vigilin. *Wiley Interdiscip Rev RNA* **8** (2017).
82. Tong, A.H. & Boone, C. Synthetic genetic array analysis in Saccharomyces cerevisiae. *Methods Mol Biol* **313**, 171-192 (2006).
83. Cohen, Y. & Schuldiner, M. Advanced methods for high-throughput microscopy screening of genetically modified yeast libraries. *Methods Mol Biol* **781**, 127-159 (2011).
84. Grote, E. Cell fusion assays for yeast mating pairs. *Methods Mol Biol* **475**, 165-196 (2008).
85. Aviner, R., Geiger, T. & Elroy-Stein, O. Genome-wide identification and quantification of protein synthesis in cultured cells and whole tissues by puromycin-associated nascent chain proteomics (PUNCH-P). *Nat Protoc* **9**, 751-760 (2014).
86. Huang, D.W., Sherman, B.T. & Lempicki, R.A. Systematic and integrative analysis of large gene lists using DAVID bioinformatics resources. *Nat Protoc* **4**, 44-57 (2009).
87. Wang, J. *et al.* In-depth method assessments of differentially expressed protein detection for shotgun proteomics data with missing values. *Sci Rep* **7**, 3367 (2017).

Figure legends

Figure 1. Systematic approach for and identification of regulators of yeast cell mating. (A) Non-biased screen for genes required for yeast cell mating. Yeast mutant libraries (knock-out and DAmP) were crossed against a WT query strain carrying a cytosolic marker fused to mCherry using the synthetic gene array (SGA) methodology. *MAT*a cells derived from the modified knock-out and DAmP libraries were then mixed with a WT *MAT*α strain that expresses a cytosolic marker fused to GFP for 3hrs. The crosses were then automatically imaged for GFP, mCherry, and mixed pattern fluorescence detection, followed by analysis. (B) Mating fraction analysis. Calculation of the mating fraction (*i.e.* percentage of cells that underwent mating) for each *MAT*a strain was determined. After thresholding and scoring, the mating fraction for each strain was calculated as the number of diploid cells (GFP/RFP) divided by the number of diploid (GFP/RFP) and haploid (RFP + GFP) cells together. After normalization (using the average mating efficiency for each plate), the mating fraction score for each mutant was plotted. A score of 1.0 designates that 100% of the *MAT*a cells underwent mating. (C) Sorted mating fraction scores. Shown are the normalized mating fraction scores for the *MAT*a mutants sorted from lowest to highest fraction. Mutants showing the most defective (lowest) and most proficient (highest) mating efficiencies were selected as genes of interest (regions highlighted in red). Mating fractions were normalized by the average mating efficiency for each plate. The grey region indicates the range of mating fraction scores obtained using WT BY4741 cells. Mutants whose scores fell within this range (0.36-0.51) were not considered for further analysis.

Figure 2. Candidate selection and validation of mutants from the mating screen. (A) Mutants with lowest mating efficiency. A partial list of mating-defective (upon mutation) genes identified from screen is given, with those having the lowest mating efficiency shown on the top. These genes encode positive regulators of mating. Genes involved in general cell transcription, translation, or metabolic processes were omitted from this analysis. (B) Manual validation of positive regulators. Quantitative mating assays were performed on the most positive regulators using manually constructed deletions/mutations to validate results of the screen. The Y axis shows the % of mating, with the mating efficiency of control WT cells (BY4741) designated as 100%. The *cdc24-m3* allele was included as a control. ORF and common names listed on the X axis indicate the mutant genes tested. **** indicates $p < 0.0001$ (C) Mutants with highest mating efficiency. A list of genes that (upon mutation) give the highest mating efficiency is shown. These genes encode negative regulators of mating. (D) Manual validation of negative regulators. Quantitative mating assays were performed for negative regulators using manually constructed deletions to validate results of the screen. The Y axis shows the % of mating, with the mating efficiency of control WT cells (BY4741) designated as 100%. ORF and common names listed on the X axis indicate the mutant genes tested. * indicates $p \leq 0.05$; ** indicates $p \leq 0.01$; **** indicates $p < 0.0001$

Figure 3. Candidate selection and validation of mutants from the mating screen using the confusion assay. (A) Schematic of the pheromone confusion assay. Left side: WT *MAT*a and *MAT*α cells normally undergo mating (*not confused*) in the absence of added α-factor (-α-factor). However, when mixed in the presence of exogenously added pheromone (+α-factor) at saturating levels they are unable to undergo directional growth towards their mating partner and fail to mate (*confused*). Right side: *MAT*a mutants of the positive regulators identified in the screen are already confused (*confused*) and, thus, show no further inhibition in mating to *MAT*α cells upon the addition of exogenous pheromone (*confused*). This indicates the relevance of the corresponding gene in gradient sensing and chemotropism. (B) Validation of chemotropism defects using the confusion assay. Confusion assays were performed on mutants previously indicated as positive regulators. Genes required for chemotropism show either no change nor decrease in mating

efficiency either with or without pheromone. Positive controls included *SCP160* lacking its KH domain (*scp160KH14Δ*), as well as *cdc24-m3*. ORF and common names listed on the X axis indicate mutant genes tested. **** indicates $p \leq 0.0001$. (C) Measure of the change in mating efficiency in cells treated with excess pheromone. The difference in mating efficiency between cells treated with exogenous pheromone (+α-factor) and untreated cells (shown in *B*) was calculated and plotted as a histogram. **** indicates $p \leq 0.0001$.

Figure 4. Relationship between activity of the MAPK pathway, cell morphology, and defects in gradient sensing. (A) Measurement of MAPK activity in the positive regulators of chemotropism and negative regulators of mating. MAPK pathway activity was measured using reporter (Fus1-GFP) gene expression in the different mutants in the presence of 5μM α-factor for 2hrs at 30˚C by flow cytometry. Reporter activity in mutants of positive regulators of chemotropism is shown on the left, while the activity in mutants of negative regulators is shown on the right. The photos (center) illustrate the activity of WT (BY4741) cells versus one of the mutants, as an example. ORF and common names listed on the X axis indicate the mutant genes tested. ns – not significant; ; *** indicates $p \leq 0.001$; **** indicates $p \leq 0.0001$. (B) Measurement of shmoo formation in the positive regulators of chemotropism and negative regulators of mating. WT and mutant *MAT*a cells were grown and treated for 2hrs in the presence of 5μM α-factor at 30˚C, prior to scoring for mating projection (shmoo) formation. The level of shmoo formation (% of cells) in the positive regulators is shown on the left, while that of the negative regulators is shown on the right. The photos (center) illustrate the shmooing of WT (BY4741) cells versus one of the mutants, as an example. ORF and common names listed on the X axis indicate the mutant genes tested. **** indicates $p \leq 0.0001$. (C) Measurement of the angle of zygote formation in the positive regulators of chemotropism and negative regulators of mating.. The zygote formation assay was applied to detect defects in gradient sensing. WT or mutant *MAT***a** cells were mixed with wild-type *MAT*α cells and incubated at 30˚C for 4hrs. The mating mixtures were then observed by microscopy. Zygotes or potential mating pairs were identified and fusion angles were determined with ImageJ: a straight line was pulled from the center of one cell to the fusion point, and then to the center of the other cell. The mean angle of orientation was $12.0^{o} \pm 1.0^{o}$ for a WT cell cross and $45.3^{o} \pm 4.1^{o}$ for a mutant cross (*e.g. ynl234w*) to WT cells. Common and ORF names listed on the X axis indicate the mutant genes tested. ns – not significant; * indicates $p \leq 0.05$; **** indicates $p \leq 0.0001$.

Figure 5. *FUS3* mRNA binding by Scp160 is modulated in an *ASC1*-dependent manner. Either wild-type (WT) cells or *asc1Δ* cells expressing FLAG epitope-tagged Scp160, both FLAG-Scp160 and $Gpa1^{Q323L}$, or FLAG-Scp160 and native Gpa1, as well as WT control cells, were grown to mid-log phase, lysed, and incubated with anti-Flag M2 affinity gel to immunoprecipitate Scp160. RNA was extracted from the TCL samples and immunoprecipitates, and used as a template for real-time qPCR. Specific primer pairs were used to detect the *FUS3* (red) and *ASH1* (grey) mRNAs. ns – not significant; ** indicates $p \leq 0.01$; *** indicates $p \leq 0.001$.

Figure 6. Scp160 binds Asc1 in a pheromone-activated manner. (A) Cells co-expressing HA-tagged Asc1 and Scp160-FLAG were left either untreated or treated with pheromone (5μM α-factor), or expressed $Gpa1^{Q323L}$ or $Gpa2^{Q355L}$ from single-copy plasmids, were used to examine the effect of pheromone pathway activation on the interaction between Asc1 and Scp160. Controls included wild-type (no tag) cells and cells expressing either HA-Asc1 or Scp160-FLAG alone. Cells were grown to mid-log phase, lysed, and incubated with anti-HA affinity gel to immunoprecipitate proteins. Samples of each immunoprecipitate (IP) were separated on a 9% SDS-PAGE gel, blotted, and probed with anti-HA and anti-Scp160 antibodies. The filled arrow indicates HA-Asc1; the open

arrow indicates Scp160-FLAG. (B) Quantification of the protein bands from (*A*) using ImageJ. A representative experiment (n=3 experiments) is shown.

Figure 7. Validation of the ribosomal protein paralog mutants identified in the mating screen. (A) Quantitative mating assays were performed on a manually constructed set of ribosomal protein gene deletion mutants identified in the screen, and which showed positive and negative effects upon mating efficiency. The Y axis designates the % of mating obtained with control WT cells (BY4741) as 100%. The names listed on the X axis indicate the mutant genes tested. ns – not significant; * indicates $p \leq 0.05$; **** indicates $p \leq 0.0001$. (B) Confusion assays to assess mating efficiency with (+) or without (-) added α-factor (5μM) at 30˚C were performed on ribosomal protein mutants previously indicated to be positive regulators. Genes required for chemotropism show either no change nor decrease in mating efficiency when treated with exogenous pheromone. **** indicates $p \leq 0.0001$.

Figure 8. Ribosomal protein paralog specificity in the translation of mating pathway-associated proteins. (A) Translatome analysis of mating-related proteins in *RPL12* and *RPL19* paralog deletion mutants. WT, *rpl12aΔ, rpl12bΔ, rpl19aΔ,* and *rpl19bΔ* cells were grown to mid-log phase in rich medium (YPD) at 30°C, prior to polysome isolation and PUNCH-P analysis (see *Methods*). After mass spectrometry, hierarchal heatmap clusters of the mating-related translatome (*i.e.* nascent polypeptide chains) was performed. Note that the *rpl12bΔ* and *rpl19bΔ* mutants cluster separately from WT and their conjugate paralog mutants (*rpl12aΔ* and *rpl19aΔ*). (B and C) Volcano plots of the mating-related nascent proteins of *rpl12aΔ* vs *rpl12bΔ* (B) and *rpl19aΔ* vs *rpl19bΔ* (C).

Supplementary Figure legends

Figure S1. Asc1 and Scp160 modulate mating in an opposing fashion. (A) Over-expression or deletion of *ASC1* affects mating. Quantitative mating between wild-type (WT; BY4742 MATα cells) and *asc1Δ* (*MAT*a; *asc1*) cells, *scp160Δ* (*MAT*a; *scp160*) cells, and WT cells over-expressing *SCP160* (*SCP160*) or *ASC1* (*ASC1*) was compared to control BY4741 (*MAT*a) and BY4742 cells (WT). The mating efficiency of the WT control cells was designated as 100%. ns – not significant; ** indicates $p \leq 0.01$; **** indicates $p \leq 0.0001$. (B) Removal of the *ASC1* intron does not affect the ability of *ASC1* over-expression to inhibit mating. To test the necessity of the *ASC1* intron, we assayed quantitative mating between wild-type BY4742 (*MAT*α) cells and either *MAT*a cells over-expressing *ASC1* lacking its intron or native *ASC1*. Crosses between BY4742 (*MAT*α) cells and either *asc1Δ* or control WT cells were performed as controls. ns – not significant; **** indicates $p \leq 0.0001$.

Figure S2. *FUS3* mRNA granule formation and localization in mating factor-treated yeast cells is controlled by Scp160 and Asc1. (A) Multiple *FUS3* granules accumulate in *asc1Δ* cells treated with α-factor. *MAT*a wild-type (WT), *asc1Δ* cells, and *scp1601Δ* cells endogenously expressing MS2 aptamer-tagged *FUS3* mRNA and co-expressing MS2-CP-GFP(x3) were grown at 30˚C on synthetic medium and treated for 2hrs in the presence of 5μM α-factor, prior to scoring for shmooing cells with visible RNA granules. Cells with either single (dark blue bar) or multiple (light blue bar) granules were scored using fluorescence microscopy. ns – not significant; **** indicates $p \leq 0.0001$. (B) *FUS3* mRNA granules are mislocalized in both *asc1Δ* cells and *scp1601Δ* cells. The mRNA granules scored in (*A*) were further examined for their intracellular localization, either to the cell body (soma; light blue) shmoo body (base; grey), or shmoo tip (dark blue). Representative images are shown. (C) *FUS3* mRNA granules are mislocalized to the cell body in both *asc1Δ* cells and *scp1601Δ* cells. Quantification of *FUS3* mRNA localization in the cells scored in (*A*). ns – not significant; **** indicates $p \leq 0.0001$. (D) Phosphorylated Fus3 protein levels are unchanged in the absence of Asc1 or Scp160. BY4741 wild-type (WT), *asc1Δ*, and *scp160Δ* cells were grown to mid-log phase and treated with 5μM α-factor for 1hr to induce *FUS3* expression. Cells were harvested and lysed for whole cell protein extraction. The lysate was separated on a 10% gradient SDS-PAGE gel and analyzed by immunoblotting with anti-pERK antibody, which detects both phosphorylated Fus3 (upper band) and Kss1 (lower band).

Figure S3. A model for translational control of the pheromone- and nutrient-sensing/filamentous growth signaling pathways during the mating response in yeast. Left panel: Glucose stimulation of the Gpr1 GPCR leads to signaling via the Gpa2 Gα subunit to activate Asc1 and Cyr1 (adenylyl cyclase)

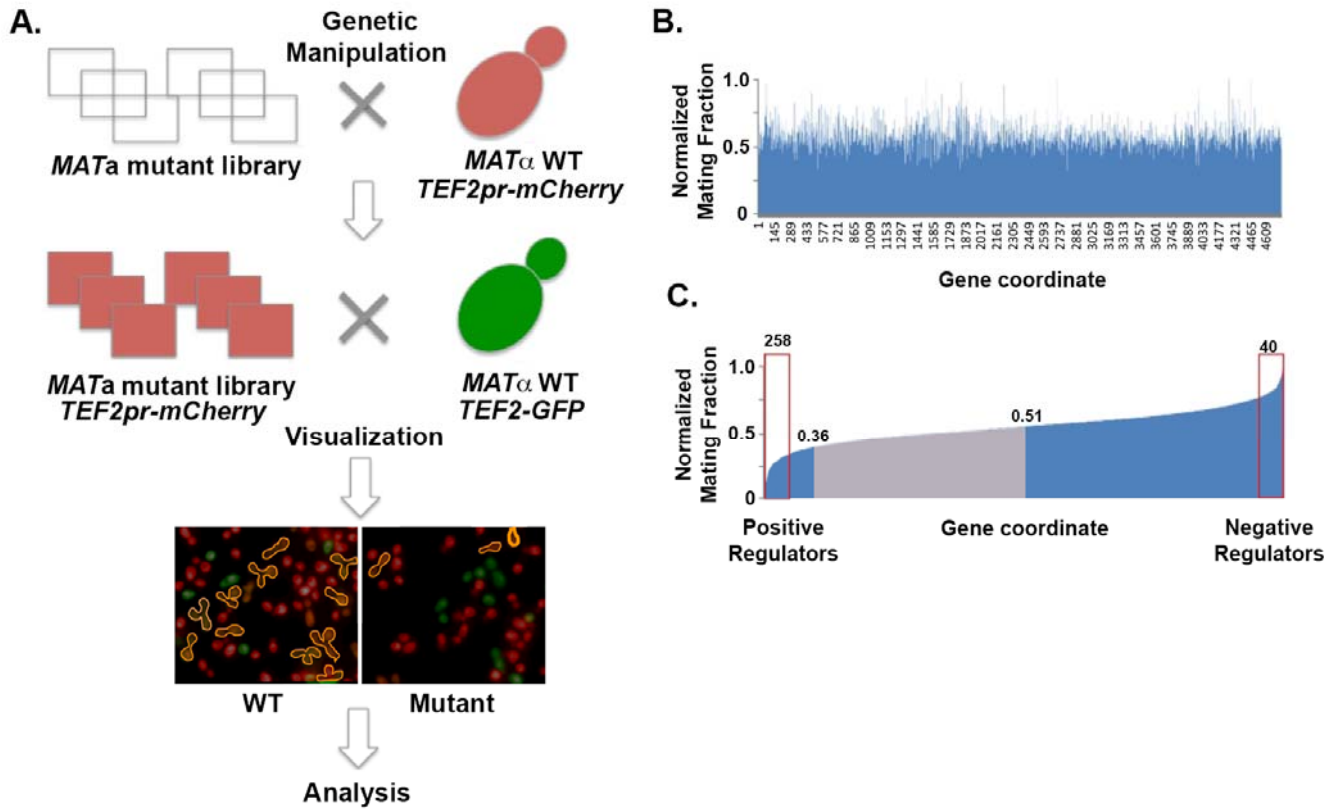
A.
Genetic Manipulation
MATa mutant library
MATα WT TEF2pr-mCherry
MATa mutant library TEF2pr-mCherry
MATα WT TEF2-GFP
Visualization
WT
Mutant
Analysis
B.
Normalized Mating Fraction
1.0
0.5
0
Gene coordinate
C.
Normalized Mating Fraction
258
40
0.36
0.51
Positive Regulators
Gene coordinate
Negative Regulators

Figure 1

A.

Normalized mating fraction	ORF	Gene Name
0.06189	YGL032C	AGA2
0.08661	YIL015W	BAR1
0.1223	YCL027SW	FUS1
0.0109	YOR219C	STE13
0.07874	YCL032W	STE50
0.1261	YBL016W	FUS3
0.18519	YJL157C	FAR1
0.0887	YML081W	TDA9
0.0653	YML082W	
0.0323	YPL161C	BEM4
0.0579	YML079W	
0.0904	YML087C	AIM33
0.111	YCR044C	PER1
0.12	YCL005W	LDB16
0.136	YMR100W	MUB1
0.167	YGR198W	YPP1
0.103	YLR262C	YPT6
0.083	YLR170C	APS1
0.287	YBR102C	EXO84
0.236	YDR349C	YPS7
0.252	YLR066W	SPC3

B.

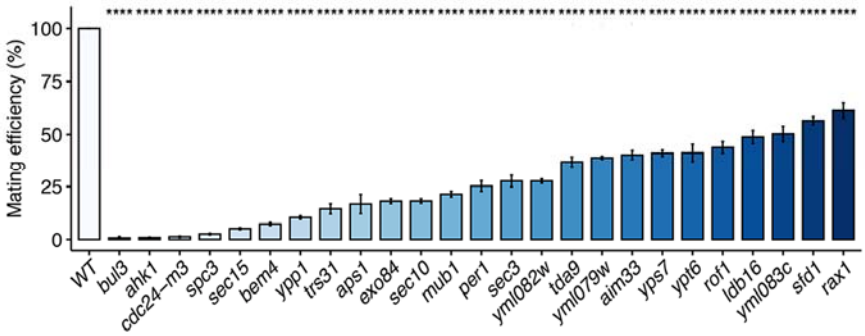

C.

0.6701	YER020W	GPA2
0.76786	YDL035C	GPR1
0.6078	YNL053W	MSG5
0.6265	YKL023W	SKA1
0.685	YJL128C	PBS2
0.7317	YLR113W	HOG1
0.683	YML053C	
0.81157	YOL081W	IRA2
0.80989	YMR116C	ASC1

D.

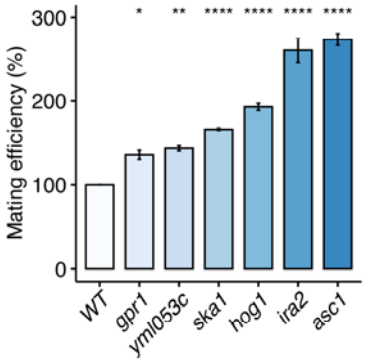

Figure 2

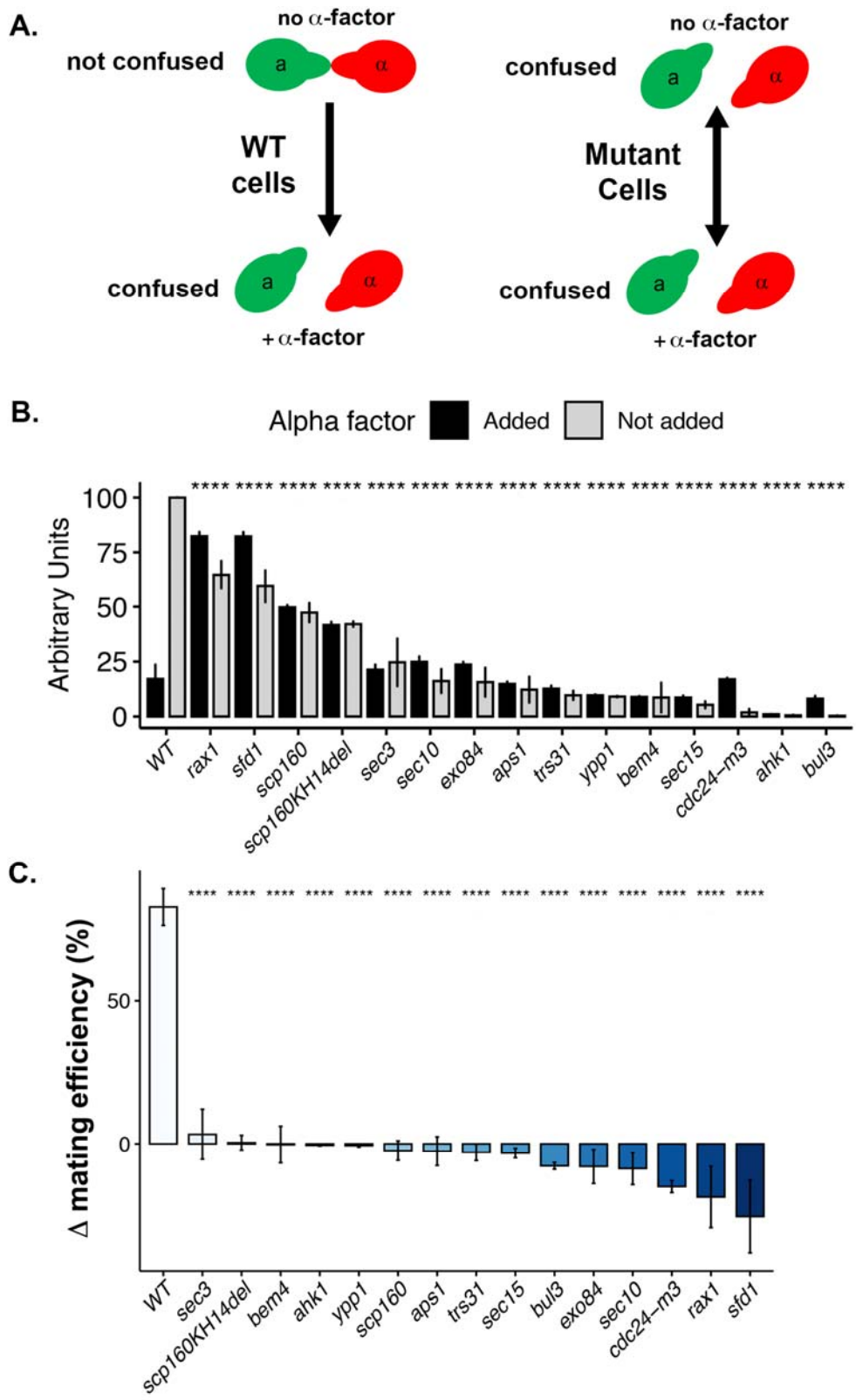
A.
no α-factor
not confused
a
α
WT
cells
confused
+α-factor
no α-factor
confused
Mutant
Cells
confused
+α-factor
B.
Alpha factor
Added
Not added
Arbitrary Units
100
75
50
25
0
WT
rax1
sfd1
scp160
scp160KH14del
sec3
sec10
exo84
aps1
trs31
ypp1
bem4
sec15
cdc24-m3
ahk1
bul3
C.
Δ mating efficiency (%)
50
0
WT
sec3
scp160KH14del
bem4
ahk1
ypp1
scp160
aps1
trs31
sec15
bul3
exo84
sec10
cdc24-m3
rax1
sfd1

Figure 3

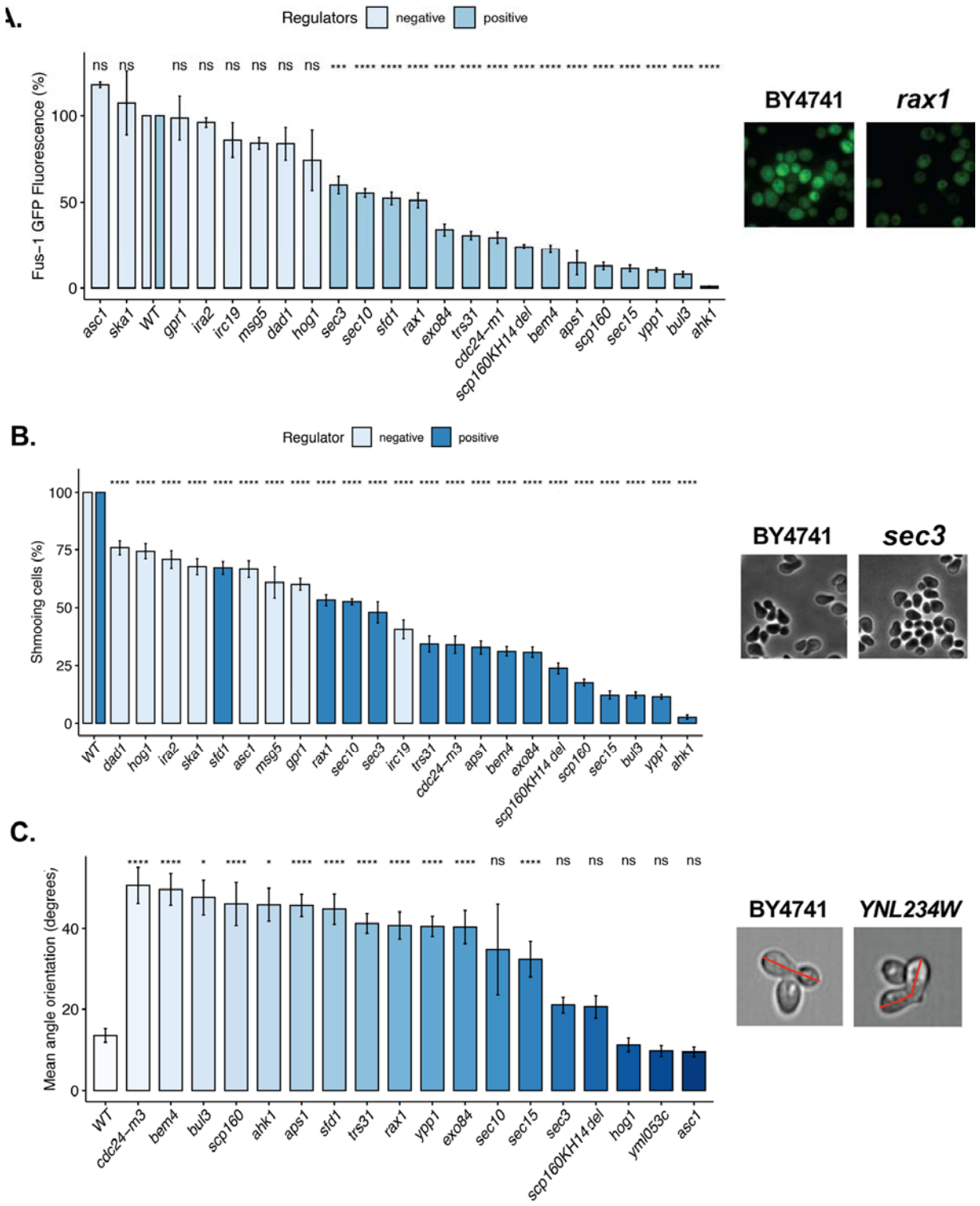
A.
Regulators negative positive
Fus-1 GFP Fluorescence (%)
asc1 ska1 WT gpr1 ira2 irc19 msg5 dad1 hog1 sec3 sec10 sfd1 rax1 exo84 trs31 cdc24-m1 scp160KH14del bem4 aps1 scp160 sec15 ypp1 bul3 ahk1
BY4741
rax1
B.
Regulator negative positive
Shmooing cells (%)
WT dad1 hog1 ira2 ska1 sfd1 asc1 msg5 gpr1 rax1 sec10 sec3 irc19 trs31 cdc24-m3 aps1 bem4 exo84 scp160KH14del scp160 sec15 bul3 ypp1 ahk1
BY4741
sec3
C.
Mean angle orientation (degrees)
WT cdc24-m3 bem4 bul3 scp160 ahk1 aps1 sfd1 trs31 rax1 ypp1 exo84 sec10 sec15 sec3 scp160KH14del hog1 yml053c asc1
BY4741
YNL234W

Figure 4

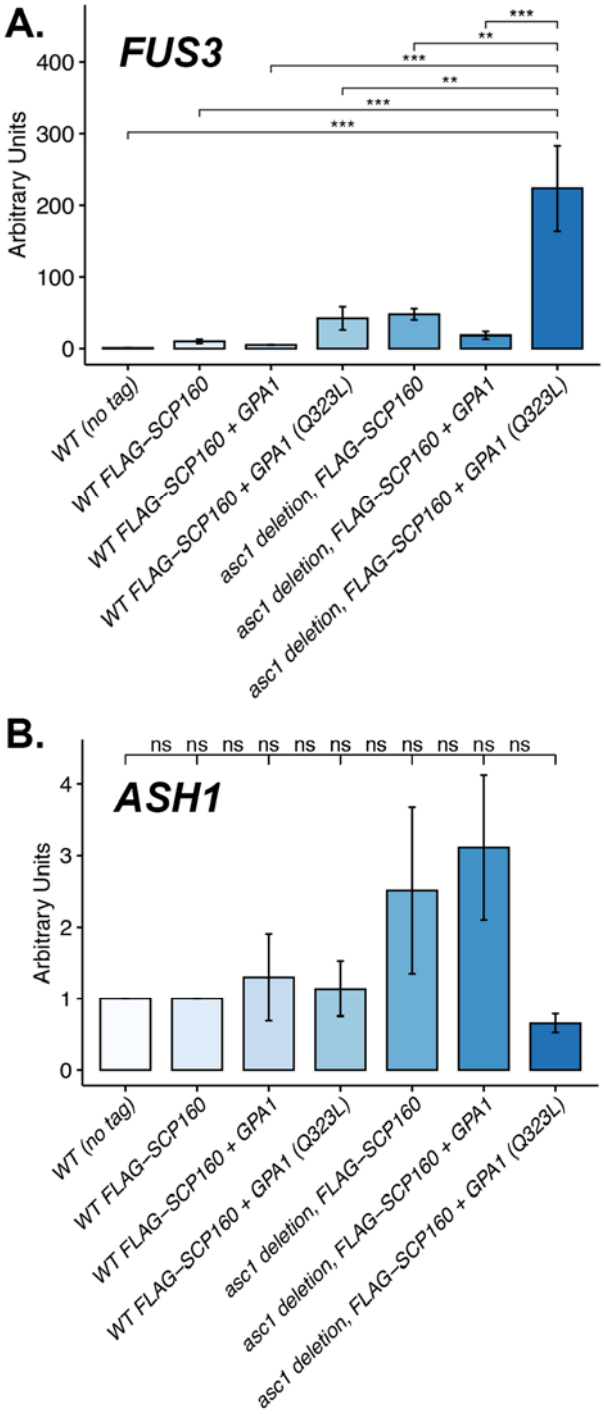
A.
FUS3
Arbitrary Units
400
300
200
100
0
***
**
***
**
***
***
WT (no tag)
WT FLAG–SCP160
WT FLAG–SCP160 + GPA1
WT FLAG–SCP160 + GPA1 (Q323L)
asc1 deletion, FLAG–SCP160
asc1 deletion, FLAG–SCP160 + GPA1
asc1 deletion, FLAG–SCP160 + GPA1 (Q323L)
B.
ASH1
Arbitrary Units
4
3
2
1
0
ns ns ns ns ns ns ns ns ns ns ns
WT (no tag)
WT FLAG–SCP160
WT FLAG–SCP160 + GPA1
WT FLAG–SCP160 + GPA1 (Q323L)
asc1 deletion, FLAG–SCP160
asc1 deletion, FLAG–SCP160 + GPA1
asc1 deletion, FLAG–SCP160 + GPA1 (Q323L)

Figure 5

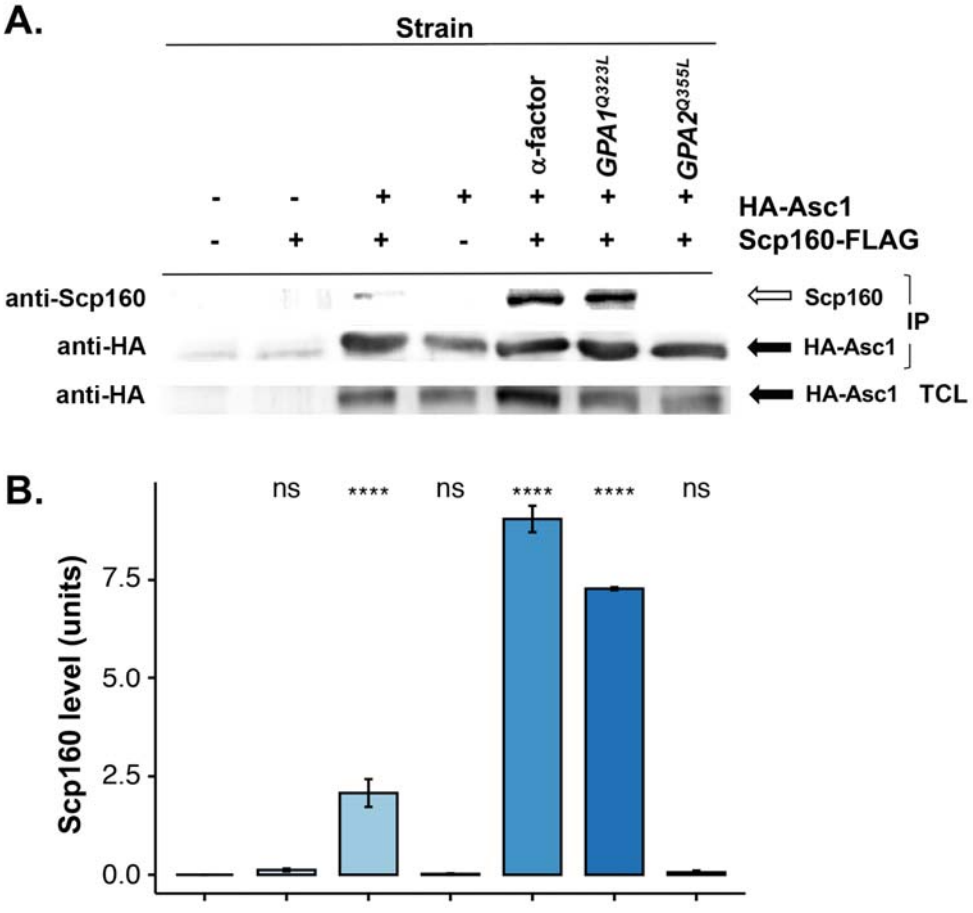
A.
Strain
α-factor
GPA1Q323L
GPA2Q355L
HA-Asc1
Scp160-FLAG
anti-Scp160
anti-HA
anti-HA
Scp160
HA-Asc1
IP
HA-Asc1
TCL
B.
ns
****
ns
****
****
ns
Scp160 level (units)
7.5
5.0
2.5
0.0

Figure 6

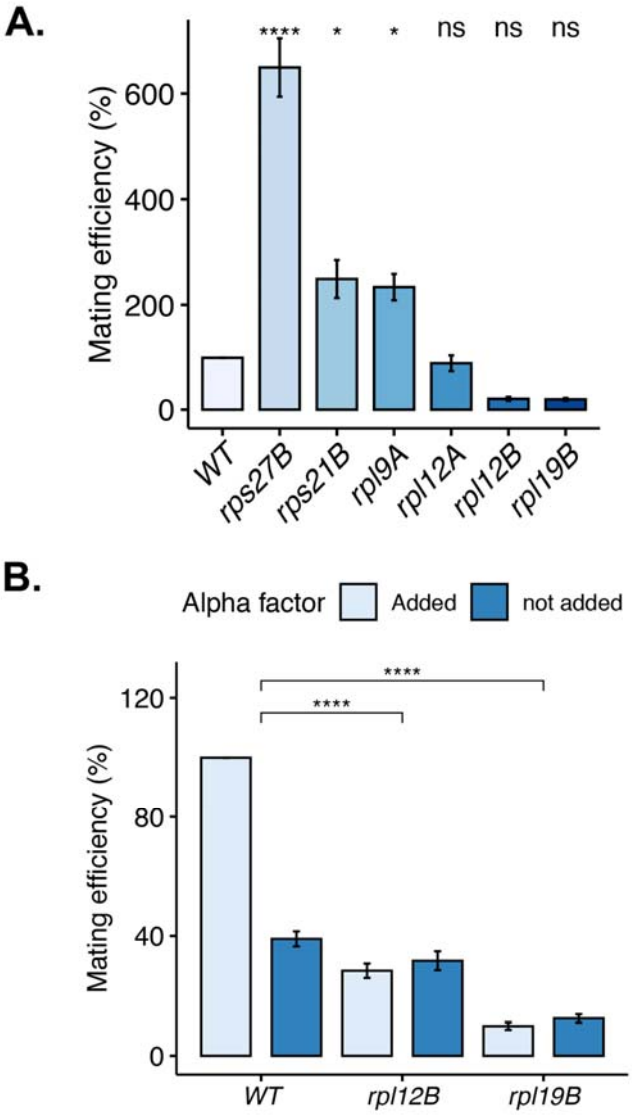
A.
****
*
*
ns
ns
ns
Mating efficiency (%)
600
400
200
0
WT
rps27B
rps21B
rpl9A
rpl12A
rpl12B
rpl19B
B.
Alpha factor
Added
not added
****
****
120
80
40
0
Mating efficiency (%)
WT
rpl12B
rpl19B

Figure 7

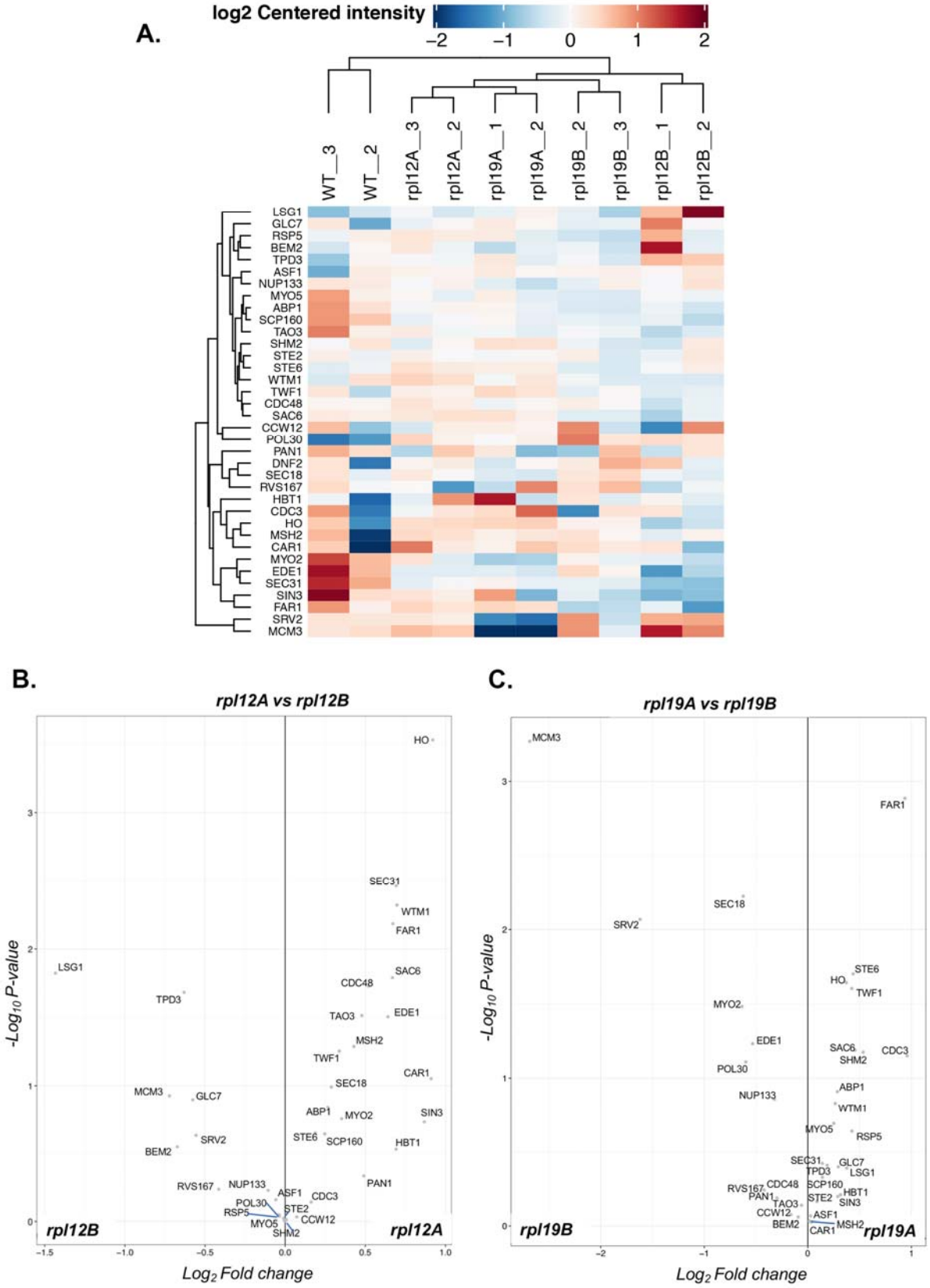
A.
log2 Centered intensity
−2
−1
0
1
2
WT__3
WT__2
rpl12A__3
rpl12A__2
rpl19A__1
rpl19A__2
rpl19B__2
rpl19B__3
rpl12B__1
rpl12B__2
LSG1
GLC7
RSP5
BEM2
TPD3
ASF1
NUP133
MYO5
ABP1
SCP160
TAO3
SHM2
STE2
STE6
WTM1
TWF1
CDC48
SAC6
CCW12
POL30
PAN1
DNF2
SEC18
RVS167
HBT1
CDC3
HO
MSH2
CAR1
MYO2
EDE1
SEC31
SIN3
FAR1
SRV2
MCM3
B.
rpl12A vs rpl12B
-Log10 P-value
Log2 Fold change
rpl12B
rpl12A
C.
rpl19A vs rpl19B
-Log10 P-value
Log2 Fold change
rpl19B
rpl19A

Figure 8

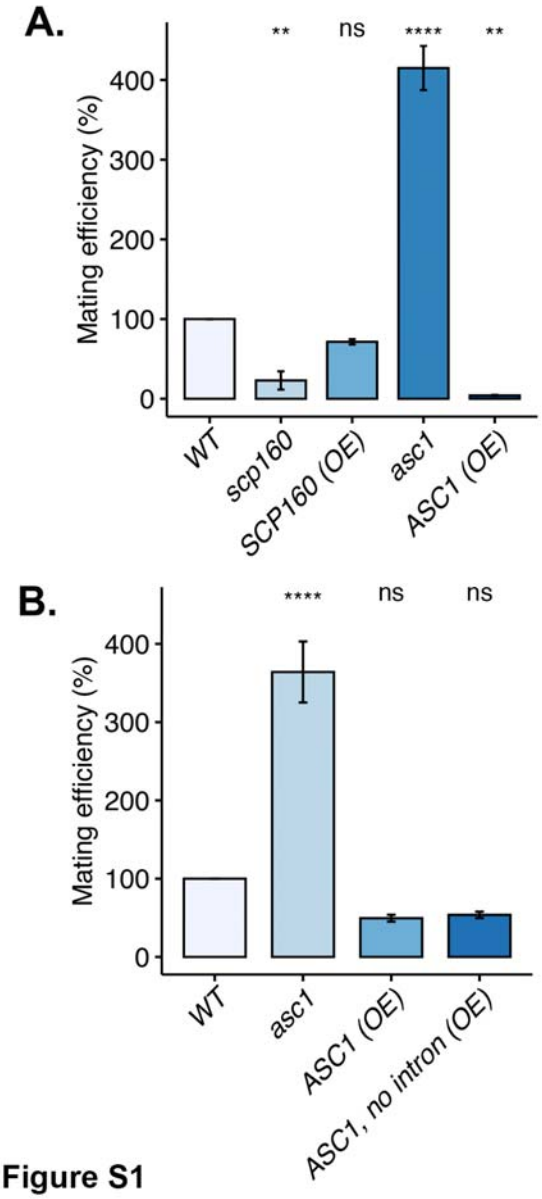
A.
**
ns
****
**
Mating efficiency (%)
400
300
200
100
0
WT
scp160
SCP160 (OE)
asc1
ASC1 (OE)
B.
****
ns
ns
Mating efficiency (%)
400
300
200
100
0
WT
asc1
ASC1 (OE)
ASC1, no intron (OE)

Figure S1

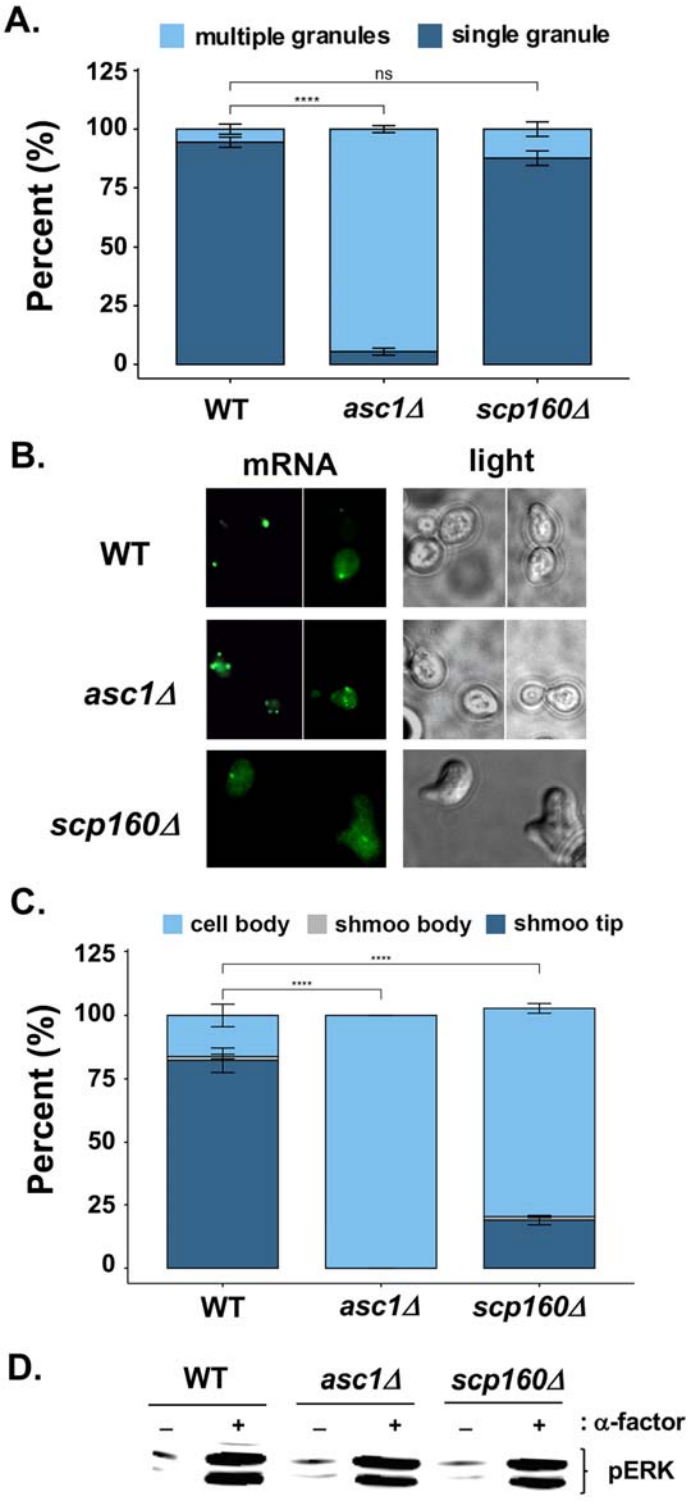
A.
multiple granules
single granule
ns
****
Percent (%)
125
100
75
50
25
0
WT
asc1Δ
scp160Δ
B.
mRNA
light
WT
asc1Δ
scp160Δ
C.
cell body
shmoo body
shmoo tip
****
****
Percent (%)
125
100
75
50
25
0
WT
asc1Δ
scp160Δ
D.
WT
asc1Δ
scp160Δ
–
+
–
+
–
+
: α-factor
pERK

Figure S2

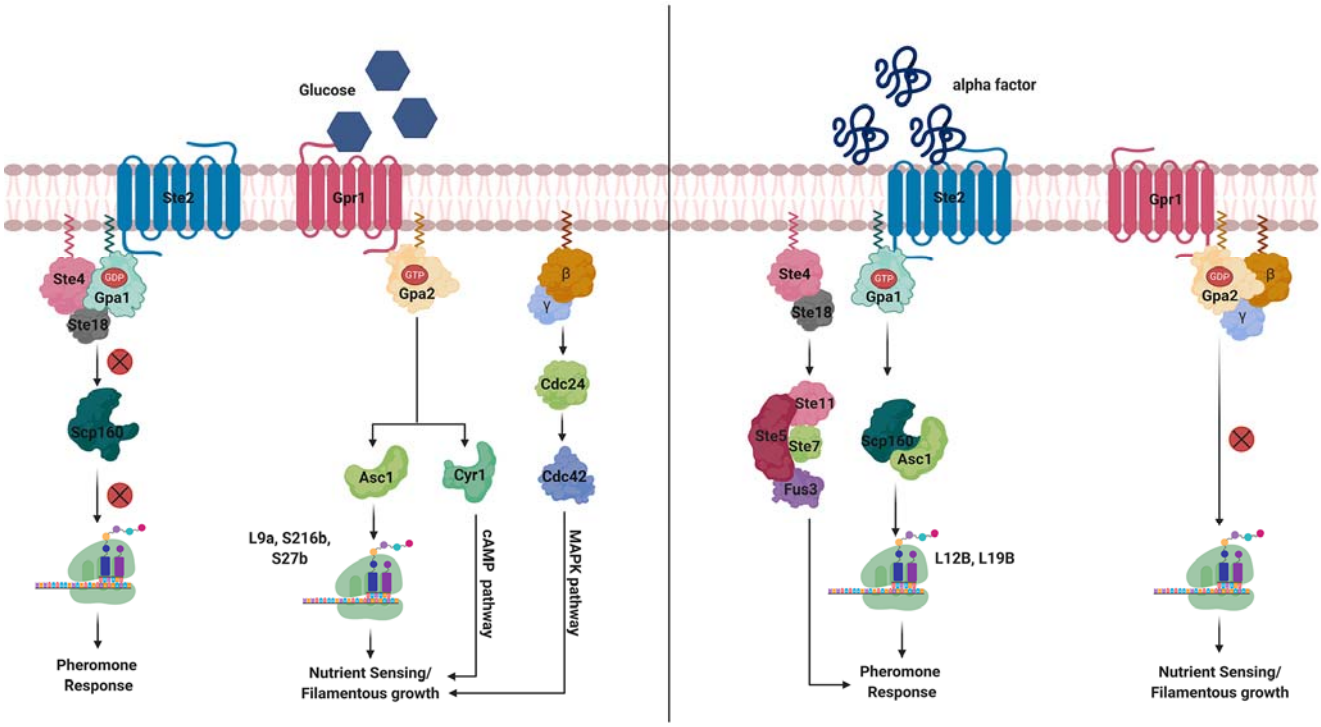
Glucose
Ste2
Gpr1
Ste4
GDP
Gpa1
Ste18
GTP
Gpa2
β
γ
Cdc24
Scp160
Asc1
Cyr1
Cdc42
L9a, S216b,
S27b
cAMP pathway
MAPK pathway
Pheromone
Response
Nutrient Sensing/
Filamentous growth
alpha factor
Ste2
Gpr1
Ste4
Ste18
GTP
Gpa1
GDP
Gpa2
β
γ
Ste11
Ste5
Ste7
Fus3
Scp160
Asc1
L12B, L19B
Pheromone
Response
Nutrient Sensing/
Filamentous growth

Figure S3

Table S2. Yeast strains

Strain	Genotype	Source
BY4741	*MAT***a** *his3Δ1 leu2Δ0 met15Δ0 ura3Δ0*	Euroscarf
BY4742	*MAT*α *his3Δ1 leu2Δ0 met15Δ0 ura3Δ0*	Euroscarf
scp160Δ	*MAT***a** *his3Δ1 leu2Δ0 met15Δ0 ura3Δ0 scp160Δ::kanMX*	Euroscarf
JFy4493 (W303)	*MAT***a** *ade2-1 his3 leu2-3 trp1-1 ura3-1 FLAG-SCP160::kanMX4*	J. Fridovich-Keil
JFy5335	*MAT***a** *ade2-1 his3 leu2-3 trp1-1 ura3-1 FLAG-SCP160KHΔ14::kanMX4*	J. Fridovich-Keil
JFy4493 *asc1Δ* (W303)	*MAT***a** *ade2-1 his3 leu2-3 trp1-1 FLAG-SCP160::kanMX4 asc1Δ::URA3*	This study
ASC1-HA (BY4741)	*MAT***a** *his3Δ1 leu2Δ0 met15Δ0 ura3Δ0 ASC1-HA::NAT*	This study
ASC1-HA (JFy4493)	*MAT***a** *ade2-1 his3 leu2-3 trp1-1 ura3-1 FLAG-SCP160::kanMX4 ASC1-HA::NAT*	This study
TEF2-Cherry SGA (S288C)	*MAT*α *ura3Δ0::TEF2pr-Cherry::URA3 his3Δ1 leu2Δ0 met15Δ0 can1Δ::STE2pr-spHIS5 lyp1Δ::STE3pr-LEU2*	M. Schuldiner
TEF2-GFP SGA (S288C)	*MAT*α *his3Δ1 leu2Δ0 met15Δ0 ura3Δ0 can1Δ::STE2pr-sp HIS5 lyp1Δ::STE3pr-LEU2 TEF2pr-GFP::NAT*	M. Schuldiner
Gene X-NAT[1] (BY4741)	*MAT***a** *his3Δ1 leu2Δ0 met15Δ0 ura3Δ0 X::NAT*	This study
FUS1-GFP (BY4741)	*MAT***a** *his3Δ1 leu2Δ0 met15Δ0 FUS1-GFP::URA3*	This study
Gene X-NAT FUS1-GFP[2] (BY4741)	*MAT***a** *his3Δ1 leu2Δ0 met15Δ0 FUS1-GFP::URA3 X::NAT*	This study

[1]The genotype of the 52 knockout strains used for manually validation (Table S1; sheet - *Manual validation*)
[2]The genotype of the wild-type and knockout mutant strains expressing *FUS1* reporter for the analysis of the MAPK pathway activity (Figure 4A)